SACLANT UNDERSEA RESEARCH CENTRE REPORT
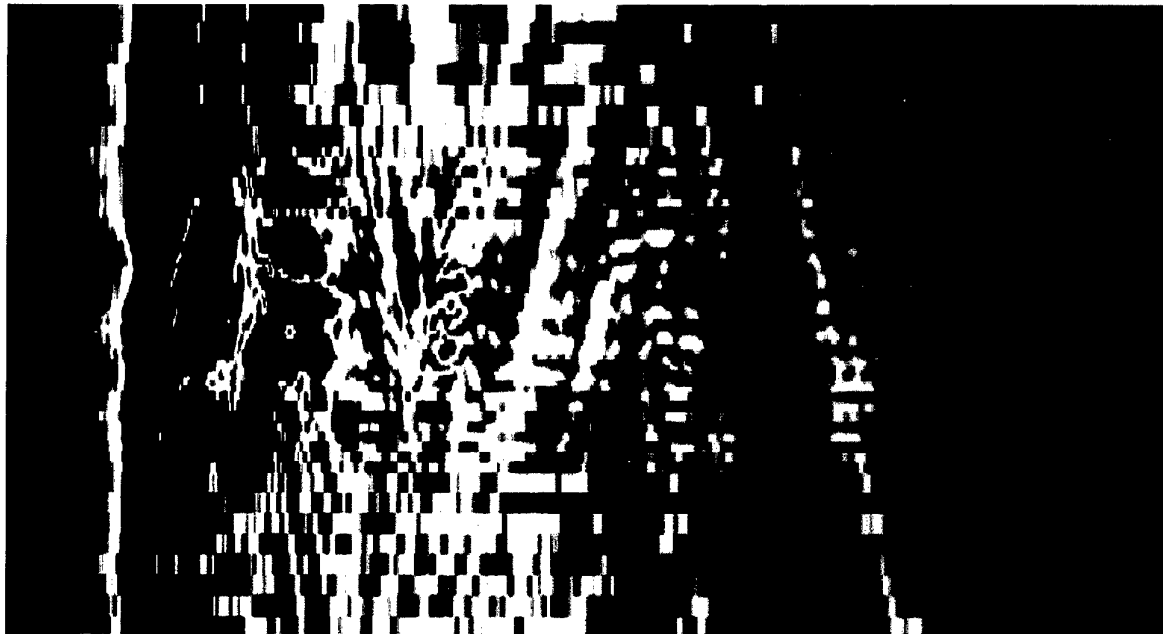

DISTRIBUTION STATEMENT A
Approved for Public Release
Distribution Unlimited

20000609 069

NORTH ATLANTIC TREATY ORGANIZATION   ORGANISATION DU TRAITE DE L'ATLANTIQUE NORD

An environmental assessment in the Strait of Sicily: Measurement and analysis techniques for determining bottom and oceanographic properties

Martin Siderius, Mirjam Snellen,
Dick Simons and Reiner Onken

Jan L. Spoelstra
Director

intentionally blank page

An environmental assessment in the Strait of Sicily: Measurement and analysis techniques for determining bottom and oceanographic properties

Martin Siderius, Mirjam Snellen, Dick Simons and Reiner Onken

Executive Summary:

In October 1997, the EnVerse 97 shallow water acoustic experiments were jointly conducted by SACLANT Centre, TNO-FEL and DERA off the coast of Sicily, Italy. The primary goal of the experiments was to test rapid environmental assessment (REA) techniques for shallow water. Most of the oceanographic REA methods discussed here are well developed and emphasis in this report is on determining the sea-bed properties through inversion of measured acoustic data. To develop an operational system, the REA techniques should be capable of identifying sea-bed characteristics over large shallow water areas. In principle, using a towed source measured on receivers at a fixed location, range dependent bottom properties along a selected track could be estimated. The research presented here describes the first steps in developing such a technique. The EnVerse 97 sound sources transmitted over a broad-band of frequencies (90–600 Hz) and the signals were measured on a vertical array of hydrophones. The acoustic data were continuously collected as the range between source and receiving array varied from 0.5–6 km. An extensive seismic survey was conducted along the track providing supporting information about the layered structure of the bottom as well as layer sound speeds. The oceanic conditions were assessed using current meters, satellite remote sensing, wave height measurements and casts for determining conductivity and temperature as a function of water depth. Geo-acoustic inversion results taken at different source/receiver ranges show sea-bed properties consistent with the range dependent features observed in the seismic survey data. Some of the issues addressed in this report are: the feasibility of towed sound source geo-acoustic inversions, applying the method to determine range dependent sea-bed properties, and the dependence of the inversions on frequency band and changing water volume.

intentionally blank page

An environmental assessment in the
Strait of Sicily: Measurement and
analysis techniques for determining
bottom and oceanographic properties

Martin Siderius, Mirjam Snellen, Dick
Simons and Reiner Onken

Abstract:

In October 1997, the EnVerse 97 shallow water acoustic experiments were jointly conducted by SACLANT Centre, TNO-FEL and DERA off the coast of Sicily, Italy. The primary goal of the experiments was to determine the sea-bed properties through inversion of acoustic data. Using a towed source, the inversion method is tested at different source/receiver separations in an area with a range-dependent bottom. The sources transmitted over a broad-band of frequencies (90–600 Hz) and the signals were measured on a vertical array of hydrophones. The acoustic data were continuously collected as the range between source and receiving array varied from 0.5–6 km. An extensive seismic survey was conducted along the track providing supporting information about the layered structure of the bottom as well as layer sound speeds. The oceanic conditions were assessed using current meters, satellite remote sensing, wave height measurements and casts for determining conductivity and temperature as a function of water depth. Geo-acoustic inversion results taken at different source/receiver ranges show sea-bed properties consistent with the range dependent features observed in the seismic survey data. These results indicate that shallow water bottom properties may be estimated over large areas using a towed source fixed receiver configuration.

Keywords: Geo-Acoustic ○ Inversion ○ Matched Field Processing ○ Range Dependent Bottom ○ Towed Source ○ Strait of Sicily ○ Adventure Bank

Contents

1
Introduction

The strong dependence of shallow water ocean acoustic propagation on sea-bed type has led to the development of inversion methods which use measured acoustic transmissions to determine properties of the bottom such as its sound speed, density and attenuation constant. Ocean acoustic inversion methods have been developed based on the technique of Matched Field Processing (MFP) [1, 2, 3, 4, 5]. For MFP inversions, a propagation code is implemented on a computer to numerically simulate the acoustic field for many hypothetical ocean environments. A search is then made for the environment that produces the best agreement between measured and simulated data. These inversions assume a geo-acoustic model of the experimental site which is made up of a number of environmental parameters. The agreement between measured and simulated data, for a particular parameter set, is quantified by an objective (energy) function. Generally the parameter search space is enormous with many local optima. Hence, efficient techniques for solving MFP inversions have been developed which use global optimization methods such as genetic algorithms and simulated annealing [2, 5, 6]. Full-field acoustic inversion results, using experimental data, have demonstrated that measurements over a broad-band of frequencies improve the bottom parameter estimates [7, 8, 9]. A collection of papers describing various full-field inversion methods are presented in [10]. The purpose of MFP inversion here is to determine a geo-acoustic model for the Adventure Bank (Strait of Sicily, Mediterranean) experimental site. This geo-acoustic model should be suitable as input to propagation codes which can then predict, for example, acoustic transmission loss, multi-path arrival structures and reverberation levels.

Experimental validation of MFP inversion methods have been applied to areas where the sea-bed was assumed to vary only with depth [9, 11, 12]. For a practical system, capabilities are needed for estimating sea-bed properties over large areas which are likely to have range and depth variability. Recently, range and depth dependent features of the sea-bed were determined from transmission loss measurements using a fixed sound source and receivers at five ranges between 8–40 km [13]. Properties of a range and depth dependent bottom may also be estimated using fixed receivers and a towed sound source. In the present paper, MFP inversion is extended to estimate sea-bed properties which vary both in range and depth by using measurements from a towed source on a stationary vertical receiving array. In principle, towed source measurements could be used for sea-bed identification over large shallow water areas and the research presented in this paper describes the first steps in

developing such a system. An added level of complexity is introduced into a towed source MFP inversion as the exact experimental geometry (i.e. relative source and receiver positions) are known with much less precision than for a fixed geometry. Since the source is moving, it is not possible to ensemble average many acoustic realizations to improve data quality (i.e. remove acoustic fluctuations due to changing water volume, changing surface roughness or ambient noise). Also, to validate the results, "ground-truth" for the sea-bed type needs to be established across the entire acoustic track. Some of the issues which will be addressed are: the feasibility of MFP inversions using a source towed over three hour periods on two different days, applying the method to determine range dependent sea-bed properties, and the dependence of the inversions on frequency band and changing water volume.

Section 2 gives an explanation of the acoustic, oceanographic and seismic data collected. The water sound speed is one of the measured oceanographic quantities which is directly incorporated into the geo-acoustic inversion. The presented ocean current data are important as they have a strong influence the vertical array position which indirectly affects the geo-acoustic inversion. Other oceanographic quantities like sea-surface temperature and wave height are presented mainly to provide a full description of the environmental conditions under which the acoustic measurements were made. The seismic data presented in Section 2 give a set of alternative measurements which help validate the MFP inversion results. The MFP inversion method is outlined in Section 3 and also, in this section, the forward propagation model is described along with the objective function and genetic algorithm optimization routine. In Section 4 the results of the MFP geo-acoustic inversion are shown which includes an estimation of the inversion quality.

2

The EnVerse 97 experiments

The EnVerse 97 experiments considered in this paper were conducted on the south end of Adventure Bank [14]. The location of the measurement systems are indicated in Fig. 1. On October 22–23, 1997 both acoustic and oceanographic measurements were taken and the following sub-sections present the collected data. Details of the acoustic data collection and processing are presented as these are directly relevant to the MFP inversion. Although most of the oceanographic and seismic data analysis are not required for MFP inversion they are presented here to fully document the experimental conditions and, where applicable, to provide "ground truth" for some of the inverted parameters.

2.1 Acoustic propagation measurements

Acoustic transmissions were made from a source towed near 50 m depth by HNLMS *Tydeman* of the Dutch Navy, with speed $\approx$ 2.5 m/s. The experiments considered here are taken from transmissions between point F and the VA where the range between source and VA was 0.5–6 km (Fig. 1). The VA was bottom moored close to NRV *Alliance*, it contained 64 receiving elements, spanned 62 m and was centered near mid-water depth. On October 22, transmissions were made using a 200–800 Hz sound projector, and on October 23, a 50–300 Hz projector was used. These will be referred to as the high frequency (HF) and low frequency (LF) sources respectively. Due to low signal to noise ratio only frequencies of 200–600 Hz will be considered for the HF source and 90–300 Hz for the LF source. The received pressure fields were first divided into snapshots of length 0.5 s for the HF data and 1 s for the LF data before Fast Fourier Transforming into the frequency domain. The length of the snapshots is determined by balancing the requirements of high signal to noise ratio and, for inversion modeling, the need to assume a fixed source position. For the inverse modeling described in Section 3, many of these snapshots are used which allows for estimating bottom properties and their uncertainty. The transmission sequences are summarized in Table 1. These 10 minute sequences contained continuous-wave, multi-tone and linearly frequency modulated signals and were repeated as the towed sources moved towards and away from the VA. In this paper, only one minute multi-tone transmissions, which occurred once in each 10 min sequence are considered. A total of four of these one-minute transmissions, two LF (at distances of 1.5 and 3.5 km from VA) and two HF (at distances of 0.7 and 2.1 km
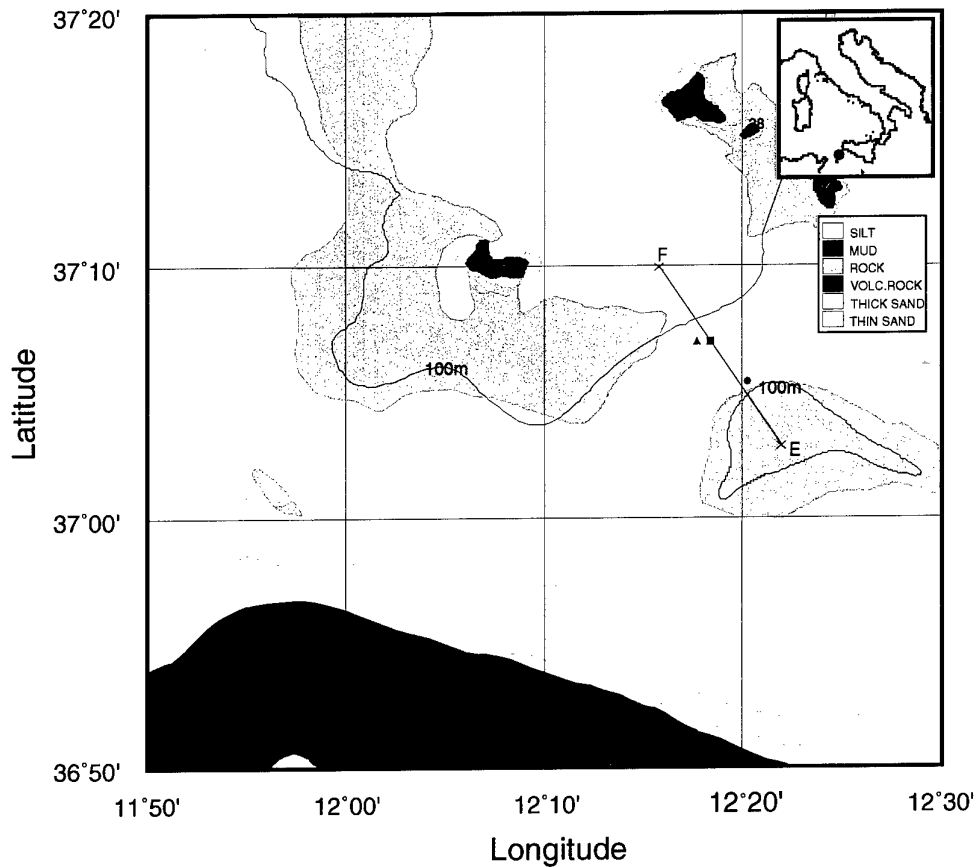
Figure 1 *En Verse 97 experimental region on Adventure Bank. Acoustic transmissions were made from a sound source towed by HNLMS Tydeman between points F and E and received on a moored vertical array of hydrophones (VA-shown as the blue square). The location of NRV Alliance (blue circle) and the current meter chain (blue triangle) are also indicated. The sea-bed types and bottom contours are taken from the SACLANTCEN geographical information system (GIS) [15] .*

Table 1 *Acoustic transmission sequences for October 22-23. Each continuous wave (CW) signal at the indicated frequencies was transmitted for 1 min. The multi-tone (MT) signals transmitted simultaneously the indicated frequencies for 1 min. Three linear frequency modulated (LFM) signals each of 1 s duration were swept over the indicated band of frequencies within the 1 min interval. The period of no transmission was used to monitor ambient noise.*

Date	Sequence time (min)	Signal type	Frequency (Hz)
October 22			
	0–6	CW	200/300/400/500/600/800
	7–8	MT	200,300,400,500,600,800
	8–9	LFM	200–800
	9–10	No transmission	
October 23			
	0–6	CW	40/55/90/130/200/300
	7–8	MT	40,55,90,130,200,300
	8–9	LFM	40–300
	9–10	No transmission	

from VA), are used in the geo-acoustic inversion. During the time to complete these one minute transmissions, the ship had sailed a total distance of about 150 m.

2.2 Oceanographic measurements

A series of oceanographic measurements were taken at the test site area. In addition to the inherent value of assessing the oceanographic conditions, these measurements and analyses are useful to determine the effects on both equipment (e.g. array tilt) and acoustic propagation. In the following sub-sections, these measurements are analyzed in conjunction with previous knowledge of this area.

2.2.1 CTD, XBT and XSV measurements

On October 22, from 14:00 to 19:00 the NRV *Alliance* made conductivity, temperature and depth (CTD) casts every 30–50 min while positioned near the VA to receive the radio telemetry. The next day, CTD casts were made at 7:02, 12:41 and 21:17 in approximately the same location. From these, the sound speeds were computed and are presented in Fig. 2. The sparse temporal resolution of these CTD casts does not permit conclusions to be drawn about the physical processes contributing to the variations, however, the overall structure of the sound speed profiles is clearly represented. The top layer (< 20 m) is homogeneous due to vertical mixing of the water

caused by surface wave motion and wind. Below the mixed layer to about 60 m there is a strong sound speed gradient which is primarily due to the water being warmed in the upper layers and is typical for summer and early fall. For comparison, a sound speed profile measured at a nearby location in October 1986 [16] and another one taken from climatology archive (NAVOCEANO GDEM [17]) are also displayed in Fig. 2. In 1986 the sound speed gradient was stronger and the sound speed was about 5 m/s higher in the top 40 m. These differences are primarily due to higher temperature in 1986. The climatology profile represents averages of temperature and salinity taken over 70 years (all in October). In comparison to both 1986 and 1997, the averaging process has weakened the gradient in the thermocline. Although the climatology sound speed captures the main features, the reduced gradient can have a strong effect on acoustic propagation. It is unlikely that a sound speed profile like the one from the climatology database would ever be found in that area. The impact of the different sound speed structure shown in Fig. 2 on acoustic propagation and geo-acoustic inversion will be investigated in Section 4.2.

Between the points F and E (Fig. 1), expendable bathythermograph (XBT) probes were deployed from HNLMS *Tydeman* every 5–10 min to determine water temperature, and expendable sound velocity (XSV) probes were cast every 10 min, while the acoustic source was being towed. Using the salinity inferred from the conductivity measurements, taken by *Alliance*, the sound speed was calculated for the XBT casts. In Fig. 3 the sound speed structure along the F-E track is shown with the main feature being the variable structure between the surface and about 40 m depth.

In general, it is unlikely that detailed sound speed profiles will always be available for acoustic forward and inverse modeling. Although useful for determining the extremes at this experimental site, the ocean sound speed was not a large factor in the outcome or quality of the geo-acoustic inversions. This is discussed further in Sections 3 and 4.

2.2.2 Current meter and sea surface temperature measurements

Information on temporal changes of the vertical structure of currents and temperature in the immediate vicinity of the vertical array is gained from a current meter mooring, which was deployed about 500 m west of the array (Fig. 1). The mooring was equipped with four current meters at nominal depths 24, 40, 55, and 70 m, recording the magnitude and direction of currents and temperature in five-minute intervals from October 22, 13:30 to October 23, 22:30. The time series of currents (Fig. 4) show that at the upper three levels the meridional component of the current is always negative, i. e. directed to the south. The mean heading at the 70-m level (-192°) is also nearly south, but here the fluctuations are stronger than above. The mean speed is steadily decreasing with depth, from 27 cm s^{-1} at the 24-m level to
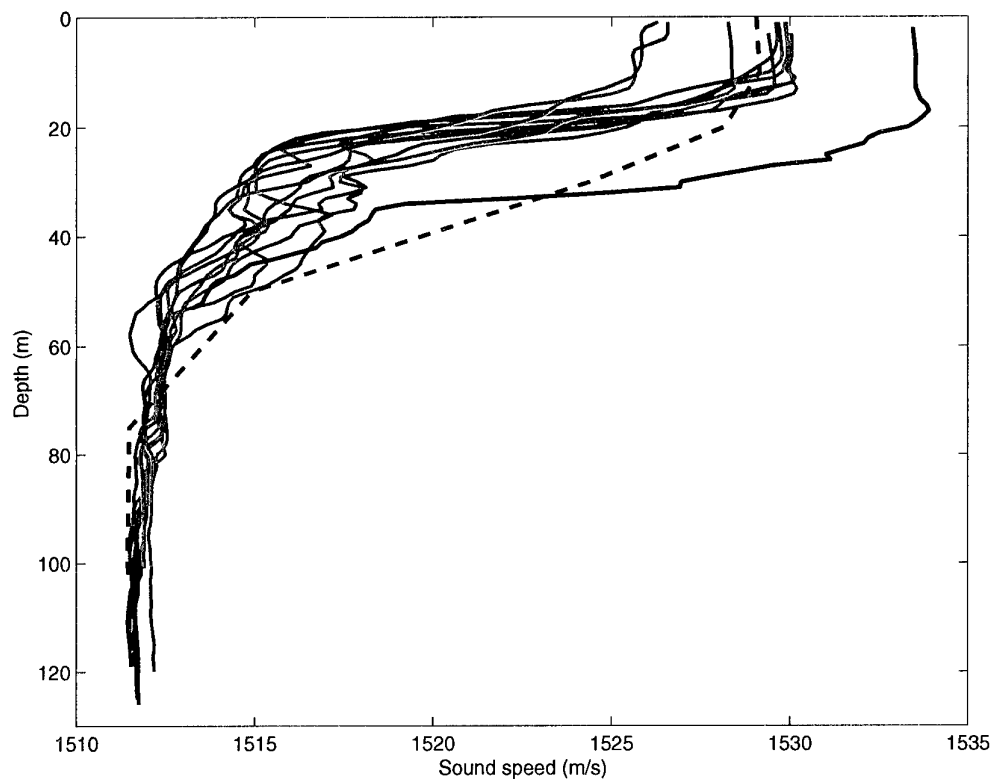
Figure 2 *Sound speed profiles for Adventure Bank. CTD measurements taken from the NRV Alliance are shown in blue and red. Blue lines indicate profiles taken every 30–50 min from 14:00 to 19:00 on October 22. Red lines are the profiles taken at 7:02, 12:41 and 21:17 on October 23. Black, dashed line is taken from the climatology database for October and black, solid line is a measured profile taken at a location near the experimental site in October 1986.*
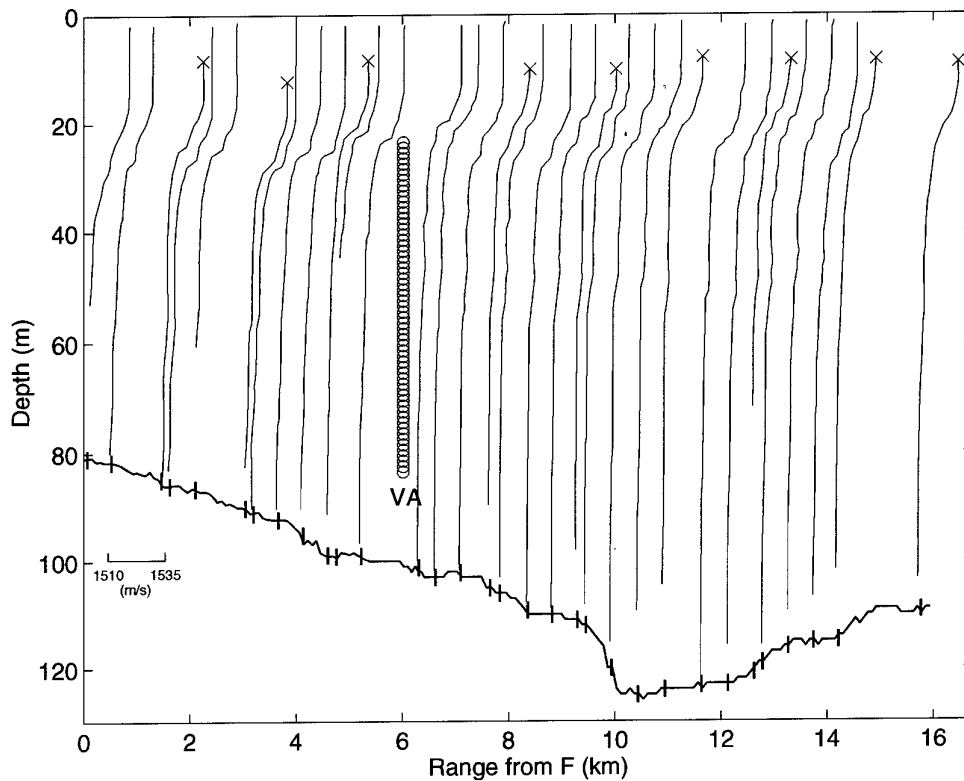
Figure 3 *Sound speed structure along F-E track taken from XBT and XSV probes deployed from HNLMS Tydeman. The XSV measurements are indicated with an 'X' on the most shallow point of the profile. The bathymetry is also shown as the solid line with tick marks indicating the location of the XSV or XBT cast. The inset scale for the sound speeds can be applied to all profiles by aligning the left edge with the tick marks on the bathymetry line. The vertical array (VA) position for October 22 is also indicated.*

6 cm s^{-1} at 20 m. At all levels, both the direction and the current speed are subject to fluctuations exhibiting a high degree of vertical coherence. It is conjectured that these fluctuations are caused by tides, but they could also be due to other physical processes, such as inertial oscillations or traveling meanders. The temperature (bottom panel of Fig. 4) is decreasing with depth and fluctuating at all levels. The fluctuations may be either caused by horizontal advection of different temperature, tides, internal waves or vertical displacements of the temperature sensors, which cannot be decided here. The fact that the amplitude of the fluctuations at the most shallow level is about 3 to 5 times greater than below is due to the larger vertical temperature gradients.

Fig. 5 displays the horizontal distribution of currents in an area located about 70 km north of the current meter mooring. Those currents were measured by a ship mounted Acoustic Doppler Current Profiler (ADCP) on-board *Alliance* over the period of time from October 21, 17:50 to October 25, 20:00 in ten-minute intervals with a vertical resolution of 8 m. In order to reduce the amount of data, the measured profiles were first vertically averaged between 18 and 90 m depth, and then the irregularly spaced data were mapped on a regular horizontal grid with mesh size 0.01° × 0.01° using two-dimensional objective analysis. This technique is widely used in meteorology and oceanography to perform a linear estimation of a scalar or vector field on a geographical grid from observational data using a minimum error variance method [18]. Fig. 5 shows a coherent pattern of strong southward flow extending at least over 10 km in zonal and about 30 km in meridional direction, and there are good reasons to assume that both the currents measured by ADCP and by the mooring farther south are part of a large scale persistent pattern of southward flow.

The latter is supported by an infrared image of sea surface temperature (SST) taken by the satellite NOAA14 on October 22. Fig. 6 shows that SST lies between 22 and 23°C over large parts of the area, however, it is up to 4°C lower offshore the southwest coast of Sicily. The cold water is found in a stripe parallel to the coast about 20 km wide, a lobe of approximately the same width extending 80 km south from the western tip of Sicily, and in a circular patch of roughly 40 km in diameter centered at about 37.4° N, 12.5° E on the eastern slope of Adventure Bank. Although it is generally impossible to draw conclusions on the horizontal flow field from SST alone, it is legitimate in this special case, because the situation is similar to those found in previous surveys. According to Refs. [19, 20], the eastern slope of Adventure Bank is the favorite site of a quasi-stationary cyclonic (counterclockwise rotating) vortex, which appears as a cold circular patch in SST due to upward bending of isotherms. Frequently, this cold patch is connected to the western tip of Sicily by a cold ribbon of SST like in the present case. The associated flow pattern is such that the currents are to first order aligned parallel to the iso-lines of SST. Hence, from the SST pattern one should expect a regime of southward flow between the Egidian Island archipelago and the site of the VA. This is consistent with the measurements.
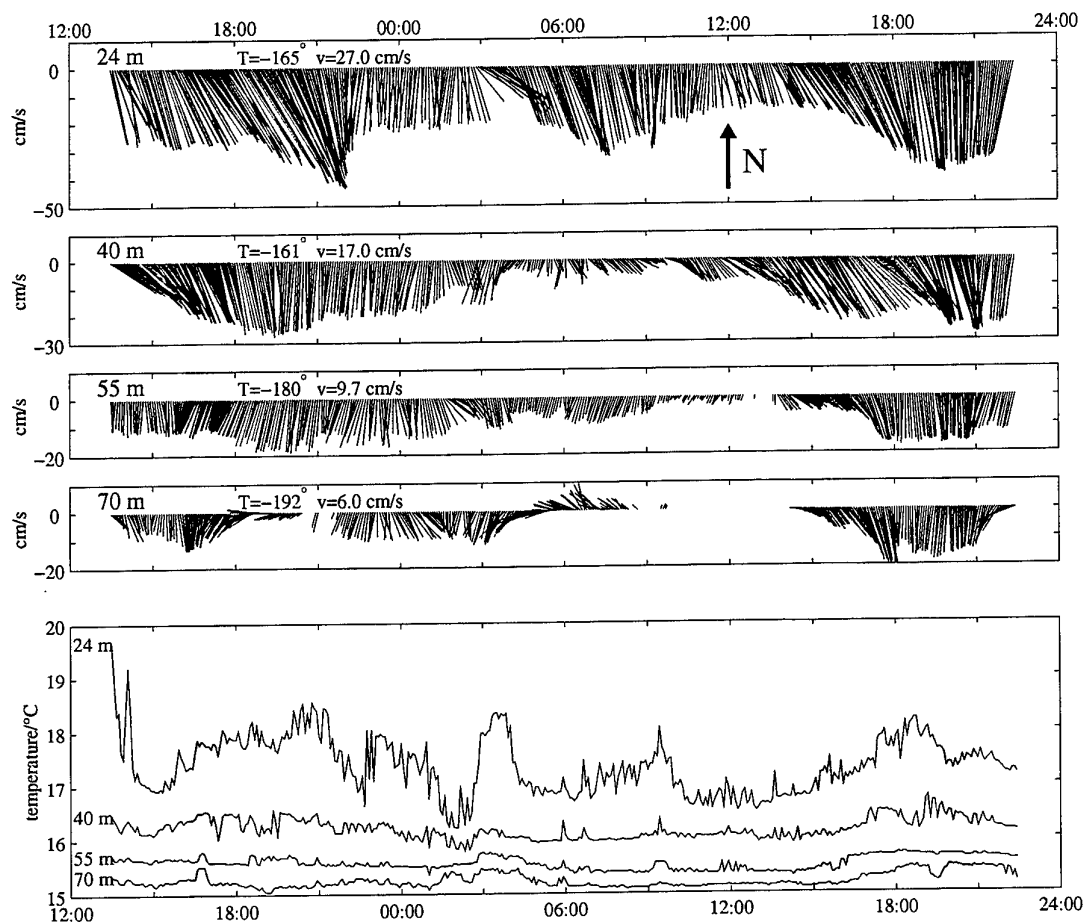
Figure 4 *Time series of currents (top panel) and temperature (bottom) of the current meter mooring positioned in the immediate vicinity of the acoustic vertical array. The nominal instrument depths of 24, 40, 55, and 70 m are indicated in each panel. T and v denote the mean direction and speed of the current averaged of the measurement period. The lower and upper limits of the time axis are October 22, 12:00 and October 23, 24:00, respectively. Measurements were taken in five-minute intervals. Left most gray shaded bar indicates the time windows of the HF acoustic transmissions and center shaded bar for the LF transmissions (data taken during the time window indicated by the right side shaded bar are not considered here).*
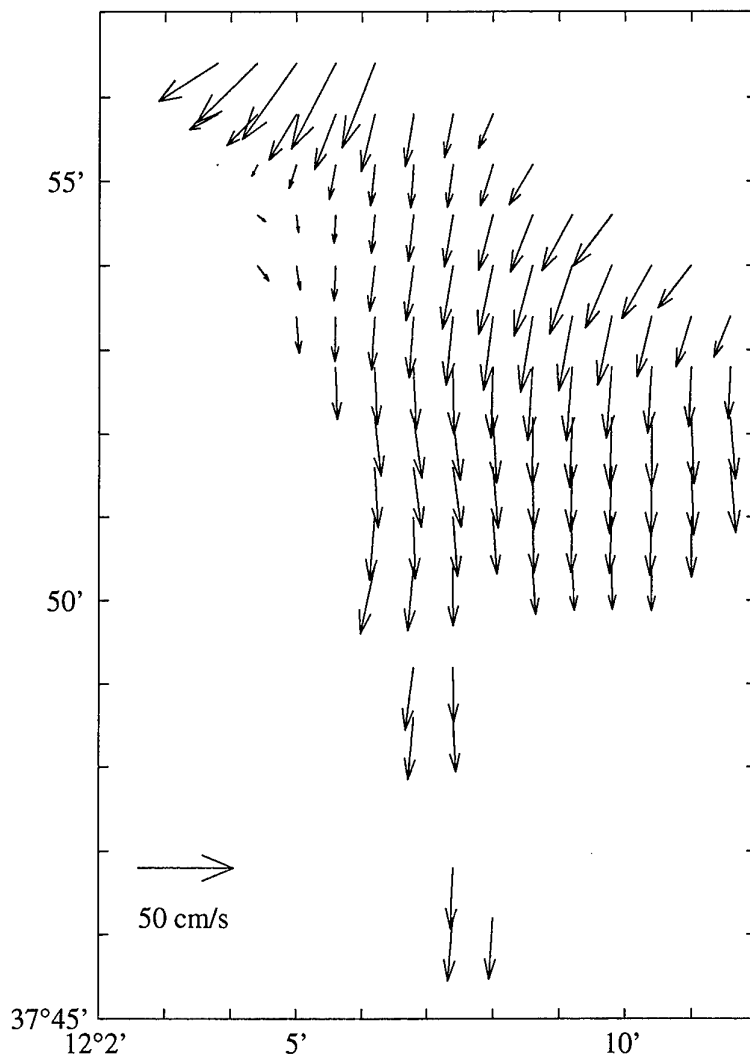
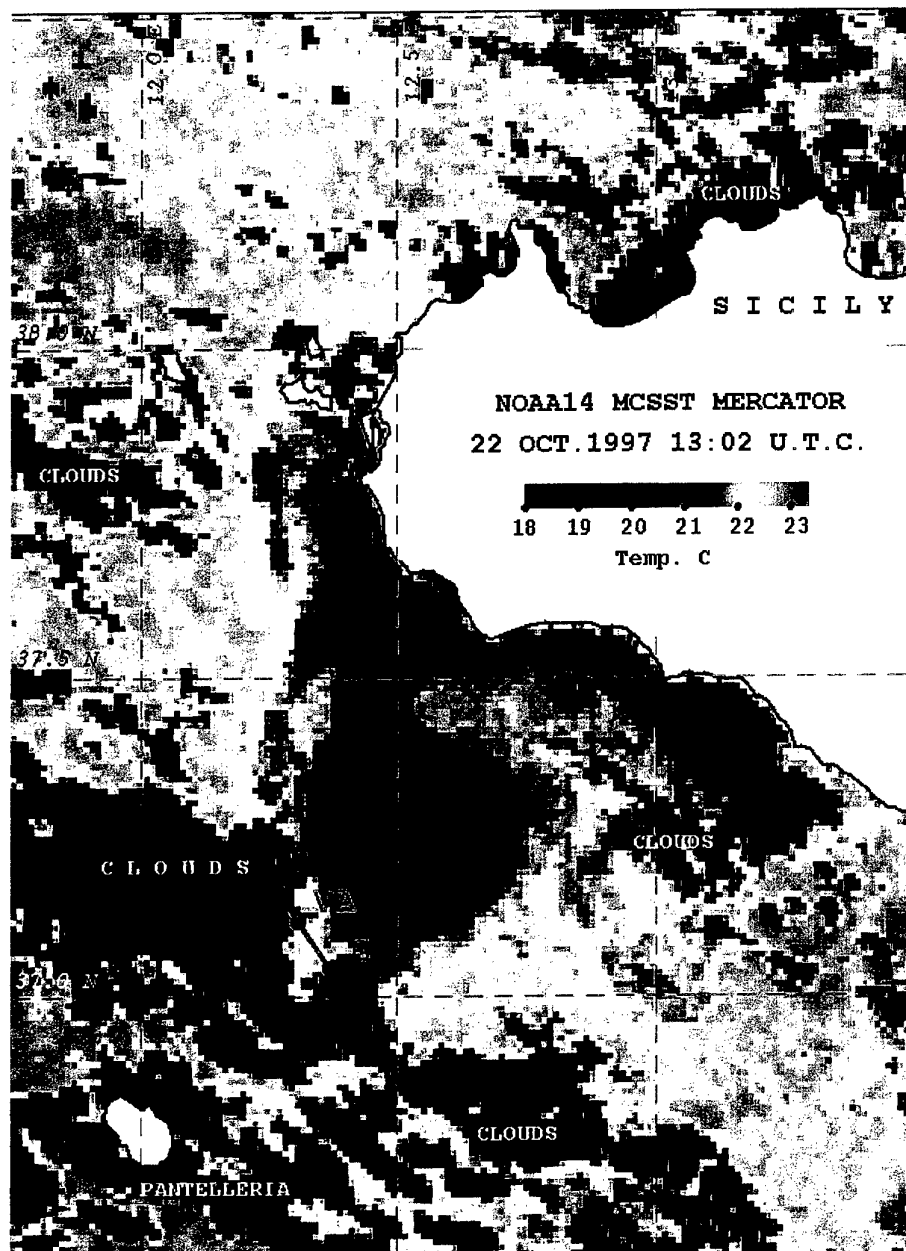**Figure 5** *Vertically averaged currents measured by ship mounted ADCP.*

Figure 6 *Sea surface temperature near the south-west tip of Sicily. The red line on the figure denotes the acoustic transmission track at points F and E with VA showing the vertical receiving array position. Note the circular region of cold temperatures to the north-east of track FE.*

2.2.3 Waverider measurements

A waverider buoy for recording surface wave heights was positioned about 35 km north-west of the VA. Figure 7 shows the spectra obtained using 20 minutes of data recorded on October 22,23 and 25. For comparison, also the JONSWAP spectrum, typical for shallow waters [21], and the Pierson-Moskowitz spectrum, typical for deep waters [22], have been determined from the prevailing wind speeds. Notice, for October 22, there is very good agreement between the spectrum determined from the data and the Pierson-Moskowitz spectrum. The spectrum on October 23 shows several peaks, indicating the presence of different surface wave fields. The high frequency part of the October 23 spectrum is also well fitted by the Pierson-Moskowitz spectrum. Other data are well fitted by the JONSWAP spectrum, e.g the data shown for October 25.

The significant wave height is calculated by taking four times the standard deviation of the waverider time series. The mean wave period T_m is determined according to:

$$T_m = \frac{\int P(f)df}{\int f P(f)df} \qquad (1)$$

where $P(f)$ is the corresponding wave height temporal-frequency spectrum. Figure 8 shows the resulting significant wave heights and the mean wave periods.

Since the significant wave heights are much less than the acoustic wavelengths used during the experiments, this is not expected to greatly impact the acoustic signals. The evolution of the acoustic signals with time on the VA are consistent with the type of changes expected for a towed source and there were not large sudden changes as might be expected if a time variable sea-surface were greatly influencing the acoustic signals or instrumentation. It is also likely that the downward refracting sound speed profile reduced sea-surface effects on the acoustics.

2.3 Seismic analysis

Seismic profiling was conducted along the acoustic track between points F and E. An impulsive broad-band signal (Boomer type source, 300 Hz–12 kHz) was transmitted and received on a ten channel horizontal towed array. The beamformed output signal was used to produce Fig. 9, which shows the bathymetry and, in colored lines, the strong reflectors due to the layers in the bottom. The layers have variable thickness ranging from 0–10 m (assuming a sediment sound speed of 1600 m/s). The squares in Fig. 9 indicate the transmission positions for the two high frequency multi-tones considered here (0.7 km and 2.1 km from VA) and the locations of low frequency transmissions are indicated by circles (1.5 km and 3.5 km from VA).
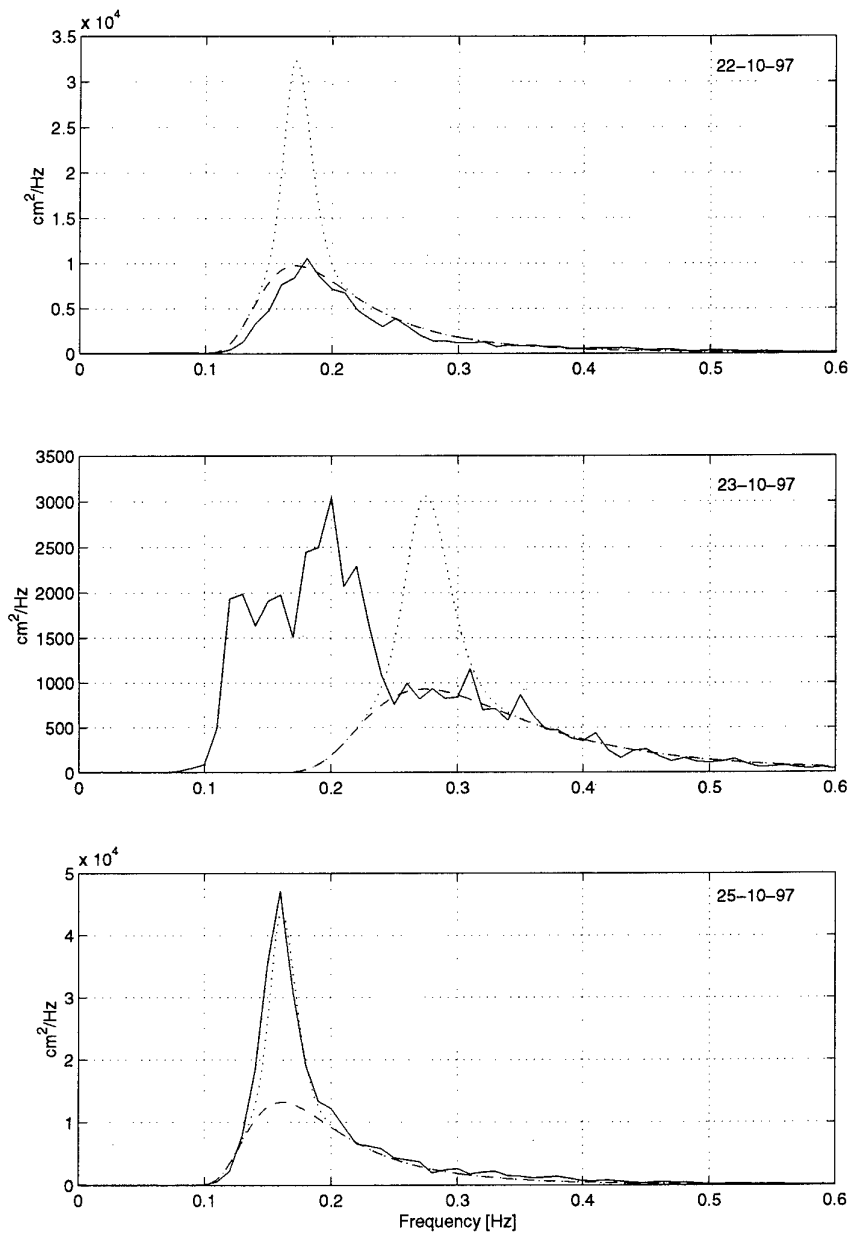
Figure 7 *Sea surface wave spectra (solid lines) as determined from 20 min of data recorded on October 22 (prevailing wind speed of 8 m/s), October 23 (5 m/s) and October 25 (8.5 m/s). Also shown are the JONSWAP (dotted line) spectrum and the Pierson-Moskowitz spectrum (dashed line), calculated from the prevailing wind speeds.*

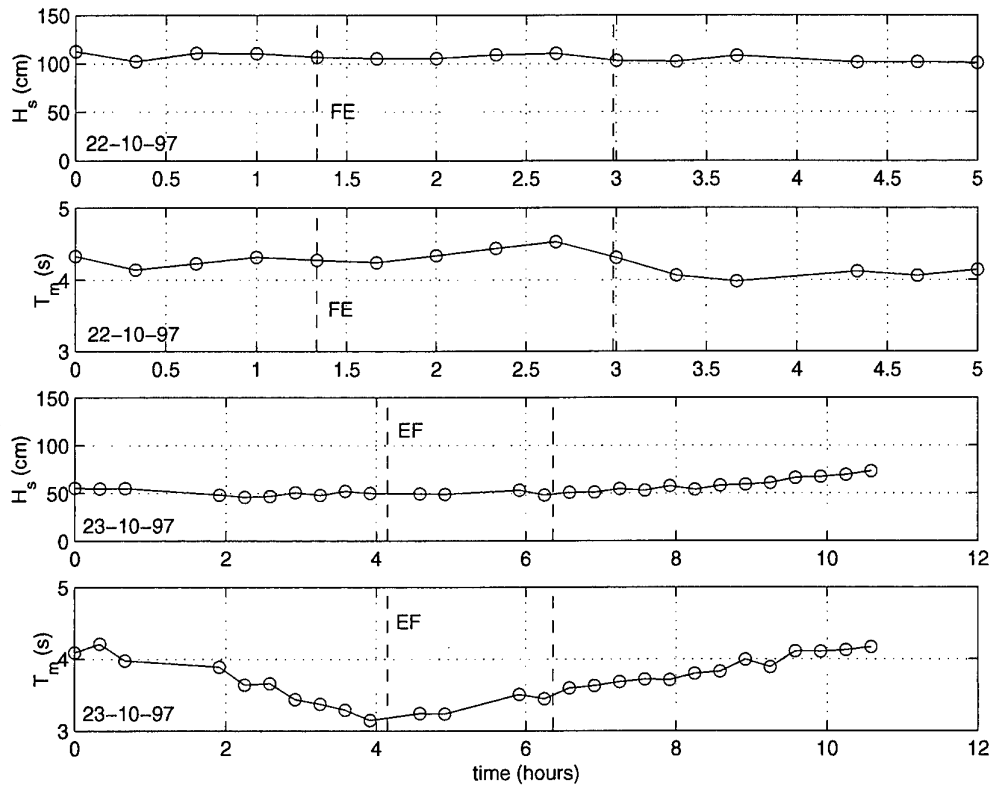**Figure 8** *Significant wave heights H_s and mean wave periods T_m calculated for each 20 minutes of data on October 22–23. Indicated with vertical dashed lines are the times during which tracks FE (HF transmissions) and EF (LF transmissions) were sailed.*
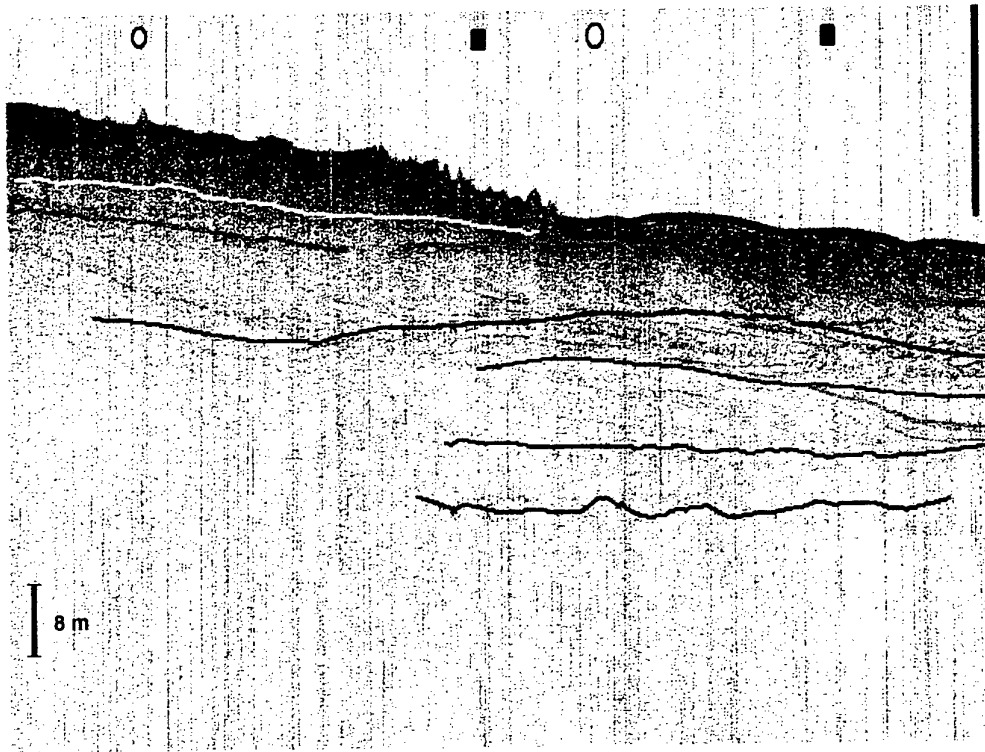
Figure 9 *The results of the seismic analysis up to 4 km north-west of the VA (towards F). The squares indicate the transmission positions for the two high frequency multi-tones considered here (0.7 km and 2.1 km from VA). The locations of low frequency multi-tone transmissions are indicated by circles (1.5 km and 3.5 km from VA). The black, vertical line on the right side of the diagram shows the VA position. In the vicinity of the VA, the first significant layer is shown as a gray line.*

2.3.1 Wide angle reflection analysis

In May 1999, a repeat seismic survey was performed over exactly the same track between points F and E (Fig. 1). A Boomer type sound source was used and the signals were received on a multi-channel streamer. This streamer consisted of eight groups of hydrophones, i.e. eight channels, and had a total length of 32 m, a group interval of 4 m and a group length of 3.8 m. Using a multi-channel streamer not only gives information on the layering in the sea-bed, but also gives information on the sound speeds of the different layers as will be explained in the following (see [23] for a more detailed explanation). Consider reflection at a certain layer. The subsurface point at which the signal, from a particular shot and received by a particular streamer channel, is reflected lies at half the horizontal distance between the source position and the position of the channel. Such points are called Common Depth Points (CDP). The source shot interval can be selected such that each CDP is shot more than once, with a maximum of n shots for a n channel streamer. Here, n is called the fold of the data. From Fig. 10 it is clear that for a n-fold coverage the firing interval should correspond to half of the distance between adjacent channels in the streamer.

Ordering the returned signals to CDP, i.e. selecting all returned signals that correspond to a particular CDP (eight in this case), results in reflections that line-up along hyperbolae. This hyperbola can be described using an analytical expression which depends on the differences in travel time from the source to the different receiver groups for the bottom reflected paths. An estimate for layer thickness and velocity is made using the analytical expression for the hyperbola which relates these quantities to the travel time.

Figure 11 shows the results of this multi-channel seismic analysis. A first reflector is identified over the entire track (at a depth ranging from 5 to 15 m). Comparing Fig. 11 from 0–4 km with Fig. 9, it can be seen that the top layers do not vary in thickness as much as indicated with the wide angle data. This is a consequence of the processing and analysis techniques used to generate these two figures. For Fig. 9, the layers are more easily identified by continuity (and then indicated with lines) once the data are lined up in range. However, with the wide angle reflection data in Fig. 11, each ping is processed to find a strong reflector, and estimate this layer velocity. Unfortunately, this allows for the possibility of a strong lower reflector to sometimes be chosen instead of an upper layer. Although this gives a false impression of the layering, the sound speed estimates are still valid and should be applied as the average sound speed in the layer (in the region above the reflector) as defined by the wide angle reflection. The mean sound speed in this first sediment layer is 1591 m/s, with a standard deviation of ±32 m/s. At the second part of the track, towards point F, a second reflector is found at an average depth of 40 m (but with, ±10 m). The second identified layer has an average sound speed of 1710 m/s ±70 m/s.
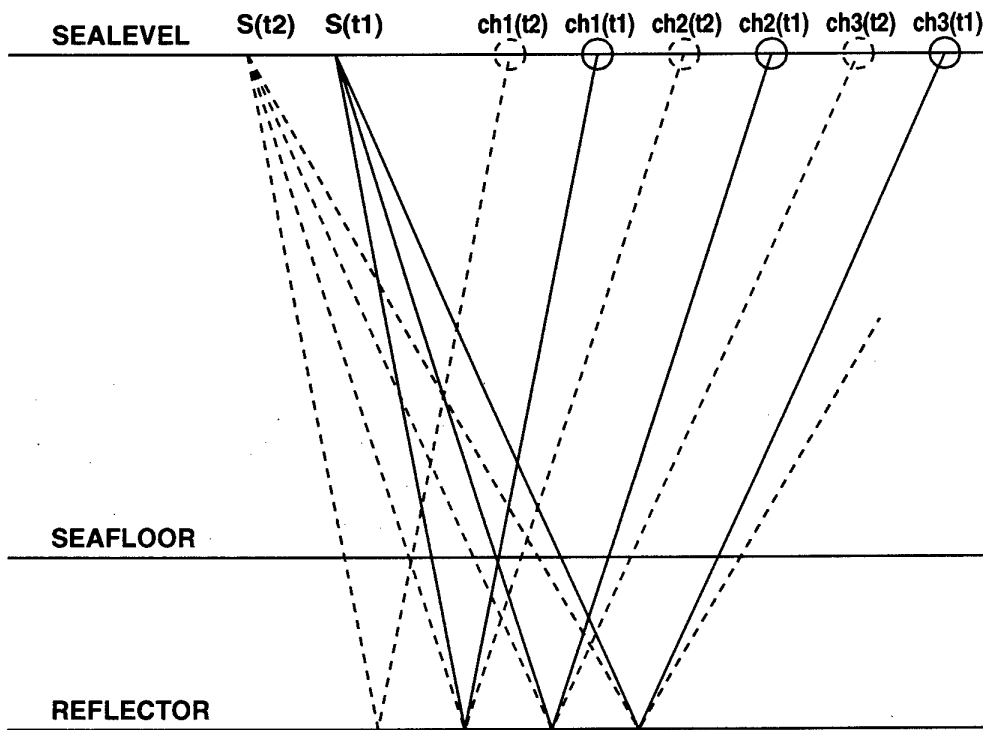
Figure 10 *Multi-channel seismic analysis. S(t1), S(t2) are the source positions at times t1 and t2, respectively. The different channels are denoted by ch1, ch2, etc. at times t1 and t2.*

Figure 11 *Multi-channel seismic analysis results: layer speeds and layer thicknesses. VA is at range 0, positive range values correspond to the North-West of the vertical array (towards point F), negative range values correspond to the South-East of the vertical array (towards point E). Top panel gives the estimated layer speed in the first and second layers. Lower panel gives the estimated thickness of the first and second layers.*

3

Acoustic inversion method

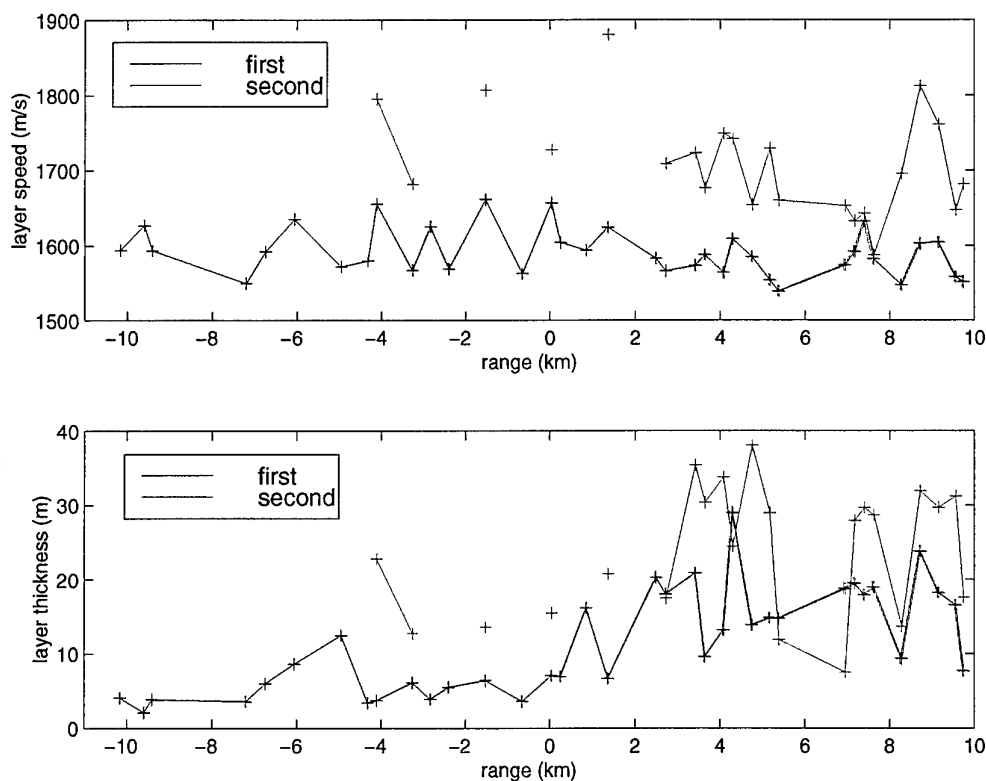The process of estimating the acoustic properties of the sea-bed by way of matched field inversion can be broken down into the following components:

- Measure the acoustic field in a given area.

- Choose a suitable forward propagation code to simulate the acoustic field.

- Parameterize the experimental site with a geo-acoustic model which can be implemented in the forward propagation code.

- Determine an objective function to quantify the agreement between measured and simulated data.

- Select an efficient algorithm to search for the set of environmental parameters (e.g. sea-bed sound speed, density and attenuation) which produces the lowest objective function value.

- After determining the environment giving the lowest objective function values, estimate the quality of the inversion (error analysis).

The previous section described the experimental measurements and the following subsections give details on the rest of the inversion process.

3.1 The forward acoustic propagation

Assume a time-harmonic $\exp(-i\omega t)$ point source in a cylindrical geometry positioned at range $r = 0$ and depth $z = z_s$. The pressure field $p(r, z)$ satisfies the Helmholtz equation and if the medium varies only with depth, the down-range solution can be found by separation of variables. In this case, the normal modes (eigenfunctions), $\Psi_n(z)$, with corresponding horizontal wavenumbers (eigenvalues), k_{rn}, satisfy the depth equation,

$$\rho(z)\frac{d}{dz}\left[\frac{1}{\rho(z)}\frac{d}{dz}\Psi_n(z)\right] + \left[\frac{\omega^2}{c(z)^2} - k_{rn}^2\right]\Psi_n(z) = 0, \tag{2}$$

where $\rho(z)$ is the density and $c(z)$ the total sound speed profile in the water and bottom layers [24, 25]. The normal mode functions and horizontal wavenumbers which satisfy (2) can be approximated by finite-difference solution techniques. Taking the outgoing solution to the range separated equation and using the asymptotic approximation for the Hankel function of the first kind, the pressure field reduces to,

$$p(r, z) = \frac{\exp(\frac{i\pi}{4})}{\rho(z_s)\sqrt{8\pi r}} \sum_{n=1}^{N} \frac{1}{\sqrt{\gamma_n}} \Psi_n(0, z_s)\Psi_n(r, z)\exp(i\gamma_n). \qquad (3)$$

Here, the near-field is not of interest so the summation in (3) is taken over a finite number of N discrete modes and the highly lossy continuous spectrum is neglected. To allow for propagation over mildly range dependent oceanic waveguides, the normal modes in (3) have been extended to functions of range and depth and γ_n represents the integration of the horizontal wavenumber over range between source and receiver [24]. This is the so-called adiabatic approximation which asserts that the modes travel independently of each other but are allowed to modify their shape and phase as they propagate to accommodate changes in the waveguide. If the medium is slightly lossy the effects are taken into account by first order perturbation theory; in this case, $\Psi_n(z)$ remains real while a small imaginary term is added to the wavenumbers, $k_{rn} = k'_{rn} + i\alpha_n$.

3.2 The geo-acoustic model for Adventure Bank

Although the seismic profiling discussed in Section 2.3 shows complicated bottom structure, a simple two layer model is often sufficient to describe the bottom acoustically. Some justification for the two layer approach can be obtained from solutions to a geo-acoustic benchmarking workshop case [26, 27]. In that benchmark case, MFP inversions of simulated data, using a two layer model, reasonably fit the properties of a multi-layer bottom in a least-squared sense. Therefore, the geo-acoustic model used here for the inversions is that of a single sediment layer overlying a sub-bottom (Fig. 12). The sound speed in the sediment is assumed to vary linearly with depth, whereas it is taken to be depth independent in the sub-bottom. The density and attenuation are assumed depth independent through both the sediment and sub-bottom. Table 2 lists each inversion parameter and the span of values in the search space.

A single water sound speed profile was chosen for each of the inversions. After some preliminary investigation, it was determined that the outcome of the geo-acoustic inversion was not greatly dependent on the particular sound speed profile chosen for the water column. Therefore, water sound speed profiles taken at times closest to the acoustic transmissions were used for the inversions.
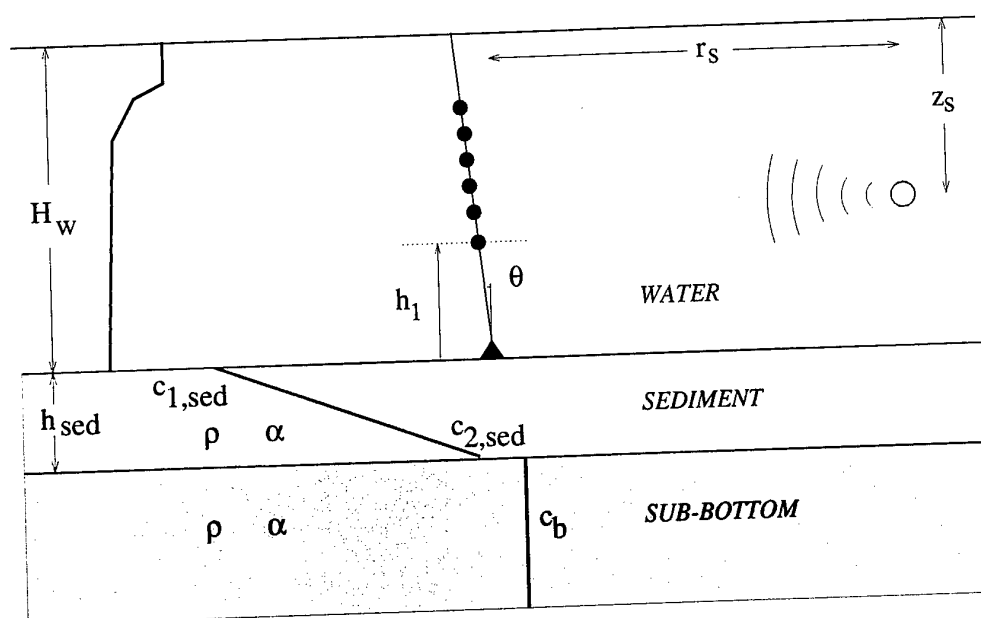
Figure 12 *The Adventure Bank geo-acoustic model and experimental configuration. Thick lines indicate, schematically, the sound speed distribution in the water, in the sediment and in the sub-bottom. For the nomenclature, see Table 2.*

Table 2 *Inversion parameters, labels and search intervals of the geo-acoustic model. Top six are geo-acoustic parameters and the bottom five are geometrical parameters. Speeds refer to compressional acoustic waves and attenuation is given in units of decibels per wavelength. The distance between VA and sound source changed for each inversion, therefore an offset distance is required to give the true search interval for r_s. The high and low frequency source range positions at 0.7-HF , 1.5-LF, 2.1-HF and 3.5-LF have corresponding range offsets of 0.0, 0.5, 1.5 and 3 km.*

Parameter Description ($\vec{m}$)	Label	Search Bounds
Sediment speed at water interface (m/s)	$c_{1,sed}$	1500–1750
Sediment speed at sub-bottom interface (m/s)	$c_{2,sed}$	1500–1800
Sediment thickness (m)	h_{sed}	1–50
Sediment and sub-bottom attenuation (dB/λ)	α	0.0–1.0
Sediment and sub-bottom density (g/cm^3)	ρ	1.0 - 2.3
Sub-bottom speed (m/s)	c_b	1515–1900
Depth of sound source (m)	z_s	20–80
Range for sound source-VA separation (+offset m)	r_s	0–2000
Water depth change from assumed value($\pm$ m)	ΔH_w	10
VA tilt ($\pm$ degrees)	θ	10
VA vertical translation ($\pm$ m)	h_1	5

3.3 Matched field objective function

The objective (or energy) function quantifies the agreement between the simulated and measured acoustic fields. The objective function chosen here is based on the incoherent multi-frequency Bartlett processor [28]:

$$E(\vec{m}) = 1 - \frac{1}{K} \sum_{k=1}^{K} |\vec{p}(f_k) \cdot \vec{p_s}^{\star}(f_k, \vec{m})|^2 \tag{4}$$

where, " $\cdot$ " indicates an inner product of the pressure vectors (over depth), $\vec{m}$ is the vector containing the parameters over which the inversion is performed, K the number of frequencies, $\vec{p}(f_k)$ the measured pressure field vector at frequency f_k and $\vec{p_s}^{\star}(f_k, \vec{m})$ the conjugated, simulated pressure field for parameter set $\vec{m}$. To obtain objective function values between 0 and 1, the inner product in (4) is divided by the normalization factor $\sqrt{|\vec{p}(f_k)|^2 |\vec{p_s}(f_k, \vec{m})|^2}$. Minimizing this energy function will lead to the parameter set corresponding to a simulated pressure field $\vec{p_s}(f_k, \vec{m})$ having maximum correlation with the measured pressure field $\vec{p}(f_k)$.

3.4 The Genetic Algorithm

The objective function given by (4) typically has many local minima. Global search methods such as genetic algorithms or simulated annealing are useful to find the optimum set of parameters corresponding to the true minimum value of (4) [5, 6, 29]. The basic principle of a genetic algorithm is as follows: First, an initial population of parameter combinations, $\vec{m}$, is created randomly; the first generation. Out of the initial population, the most fit members (i.e. those with the lowest objective function value) have the highest probability to be selected as "parents". From the parents, "children" are obtained by the operations of crossover and mutation. The crossover operation can, with probability $1 - P_x$ duplicate one of the parent's parameters in $\vec{m}$, or, with probability P_x perform a bit crossover of the two parents. That is, using bit string representations of the parameter values, form the child's string by taking part from one parent and part from the other. The mutation operation makes a change of a single bit in the parameter value string to allow for better exploration of the parameter space. Part of the children are then used to replace the least fit members of the initial population creating the next generation. Successive generations become increasingly fit and the process is continued until the optimization process has converged.

3.5 Quality of the inversion results

Estimates for the optimum values of the parameters can be derived from the members of the final genetic algorithm population. This can be done by taking the parameter combination with the lowest energy function value. This solution to the inverse problem will be referred to as GA_{best}. An alternative method is to calculate the so-called *a posteriori* mean values [5]. These are given by,

$$GA_{mean}(\vec{m}) = \sum_{j=1}^{J} \vec{m}_j \, \sigma(\vec{m}_j) \tag{5}$$

with

$$\sigma(\vec{m}_j) = \frac{exp[-E(\vec{m}_j)T^{-1}]}{\sum_{i=1}^{J} exp[-E(\vec{m}_i)T^{-1}]}. \tag{6}$$

The summations in (5), (6) are over J solutions from the final GA populations, where, J is the product of the population size with the number of independent GA runs (here, $J = 64 \times 5 = 320$). Following [5], T is set equal to the average of E over the 50 best members. Generally, it is useful to calculate both GA_{best} and GA_{mean}, since a significant difference between these two indicates either a flat or ambiguous distribution and the parameter value is not well determined.

An estimation of the errors can also be obtained by evaluating inversions for several snapshots of the one minute multi-tone data sets. Although the source was moving during the transmissions, it is assumed that changes in the bottom properties are negligible over this short distance. Therefore, by inverting many snapshots, an estimate of the uncertainty in the results can be made. The mean of the GA_{best} solutions taken over snapshots of data is used to estimate the parameter value and the standard deviation to estimate the error. At least nine snapshots were used for each inversion to make these estimates.

4

Results and analysis

Matched field inversion, using the method outlined in Section 3, was used to determine the bottom properties for the Adventure Bank site at the four range positions. Figure 13 shows the inversion results for the different snapshots of high frequency data (HF) at the 0.7 km range position. At each of the four range positions (HF-0.7 km, LF-1.5 km, HF-2.1 km, LF-3.5 km) similar sets of inversion results were produced for all the snapshots of data. These results are put in summary form in Table 3 for the geometrical parameters and Table 4 for the geo-acoustic parameters. Presented in these tables are the average and standard deviation for $\mathrm{GA_{best}}$ values taken over all inverted snapshots of data at each range.

4.1 Assessment of the inversion results

A comparison between $\mathrm{GA_{best}}$ and $\mathrm{GA_{mean}}$, for any single snapshot of data, gives insight into the quality of the inversion. For a given parameter, a large difference between these two indicates a flat or ambiguous distribution of values (i.e. several peaks all with low objective function values). Whereas, agreement is an indication that there is one sharply peaked minimum. With this criterion, it was ascertained that the geometrical parameters and $c_{1,sed}$ were well determined for nearly all snapshots. Parameters $c_{2,sed}$ and c_b are not as well resolved and h_{sed}, α and ρ even less. This essentially gives an indication of the sensitivity of each of the inverted

Table 3 *Geometrical parameter estimates for inversions at 0.7, 1.5, 2.1 and 3.5 km. The results are the average and standard deviation for $\mathrm{GA_{best}}$ values taken over all inverted snapshots of data at each range. Differences from the direct measurements of source range (r_s), source depth (z_s), water depth (H_w), array tilt (θ) and array translation (h_1) are indicated as Δr_s, Δz_s, ΔH_w and $\Delta\theta$ and Δh_1.*

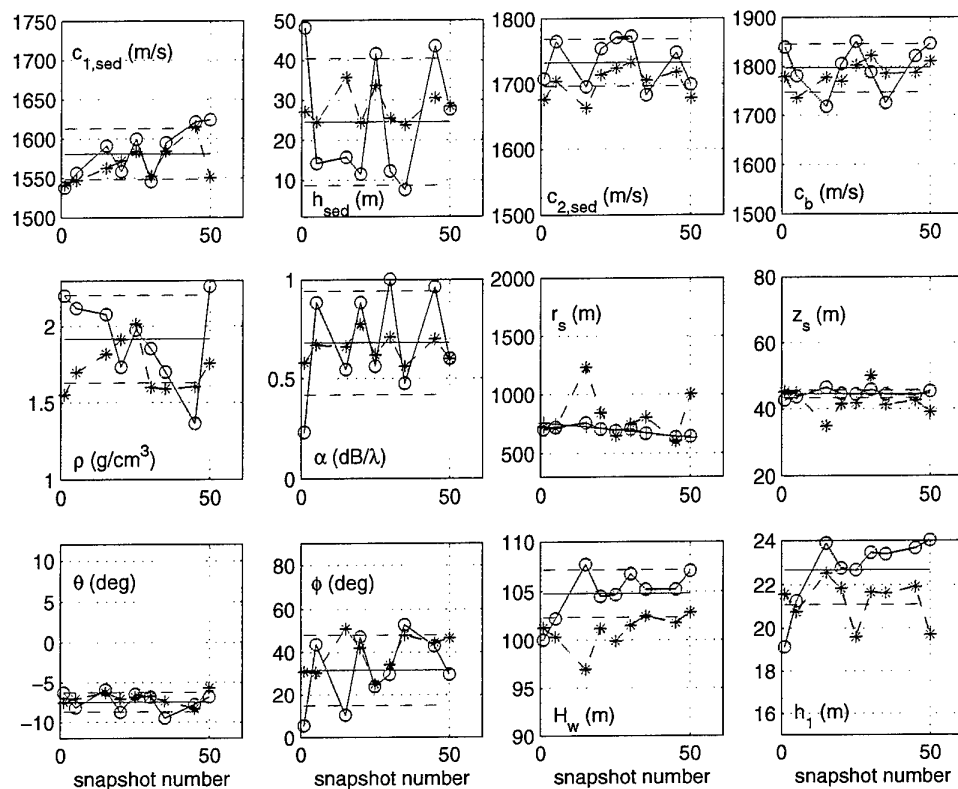| Range-Band	Δr_s (m)	Δz_s (m)	ΔH_w (m)	$\Delta\theta$ (deg)	Δh_1 (m)
0.7 km, HF	-2.9 ± 26	-2.5 ± 1.1	4.8 ± 2.4	-0.4 ± 1.2	1.2 ± 1.6
1.5 km, LF	58 ± 72	1.8 ± 1.9	0.5 ± 2.1	0.5 ± 1.1	3 ± 0.8
2.1 km, HF	40 ± 21	-4.8 ± 0.4	2.8 ± 0.8	-1.8 ± 1.1	0.5 ± 1.0
3.5 km, LF	105 ± 280	-4.2 ± 1.3	1.7 ± 5	0.1 ± 1.0	2.2 ± 2.3

Figure 13 *The inverted parameter values for the high frequency source (HF) at the 0.7 km range position. Each of the circle/star values represents the result of inverting 0.5 s of data. The circles denote the* GA$_{best}$ *solutions, and the stars denote* GA$_{mean}$ *results. The solid green lines are the mean values of* GA$_{best}$ *and the dashed lines indicate the* GA$_{best}$ *standard deviation. The red line on the* r_s *plot shows the estimated source range position using ship's navigation. The y-axes indicate the search bounds.*

Table 4 *Geo-acoustic parameter estimates for inversions at 0.7, 1.5, 2.1 and 3.5 km. The results are the average and standard deviation for* GA$_{best}$ *values taken over all inverted snapshots of data at each range.*

Range-Band	$c_{1,sed}$ (m/s)	$c_{2,sed}$ (m/s)	c_b (m/s)	h_{sed} (m)	α (dB/λ)	ρ (g/cm^3)
0.7 km, HF	1580 ± 32	1732 ± 36	1797 ± 49	25 ± 16	0.68 ± 0.26	1.92 ± 0.29
1.5 km, LF	1641 ± 16	1746 ± 46	1813 ± 51	31 ± 12	0.43 ± 0.16	1.46 ± 0.18
2.1 km, HF	1572 ± 63	1733 ± 44	1805 ± 45	5.7 ± 2	0.92 ± 0.11	1.62 ± 0.13
3.5 km, LF	1576 ± 33	1749 ± 47	1840 ± 62	11 ± 5	0.91 ± 0.08	1.28 ± 0.17

parameters. Lower sensitivity indicates that the parameter value is more difficult to extract and therefore is less significant with respect to acoustic propagation. The standard deviations in Tables 3, 4 give a more quantitative estimate of the errors associated with each inverted parameter value.

4.1.1 Analysis of the geometrical parameter estimates

In general, for all inversions, the geometrical parameters (r_s, z_s, H_w, θ and h_1) are well determined as indicated by the agreement between GA_{best}, GA_{mean} and their relatively low standard deviations. This is not a surprising result since, typically, altering the geometry causes large changes in the down-range pressure field which consequently impacts eq. (4). For this reason, the geometrical parameters usually converge quickly. Since the geometry of the experiment is known from direct measurements, comparing this with the inverted geometry is a valuable sanity check of the entire inversion process. For convenience, the differences between measured and inverted geometry values Δr_s, Δz_s, ΔH_w, $\Delta\theta$ and Δh_1 are listed in Table 3. The source range has been estimated using a Differential Global Positioning System (DGPS) on-board HNLMS *Tydeman* (plus offset for the tow cable distance) and the value is in good agreement with the inversion results. This position is indicated by a red line on the r_s plot in Fig. 13. The source depth was approximated by a pressure sensor on the tow-body and, on October 22, was 47 ± 2 m and on October 23, 50 ± 2 m. These z_s values are also consistent with the inversion results. The VA position (i.e. depth of the hydrophones) from the inversion agrees well with that measured before deployment on October 22 and 23. The bathymetry taken from echo-soundings and presented in Fig. 3 is range dependent with water depth about 100 m near the VA. The inversion results for ΔH_w are within acceptable limits of the known bathymetry (i.e. < 5 m).

4.1.2 Analysis of the array tilt estimates

Two methods were used to estimate the VA tilt (θ). The first method uses the matched filtered output of linear frequency modulated (FM) signals transmitted within one min of the multi-tones used for inversion. The FM signal was one second in duration and swept the band 200–800 Hz (Table 1). On October 22, 1997, in total nine FM sweeps were transmitted at distances of ≈ 0.5, 2 and 3.6 km from the VA. Figure 14 shows, for these three distances, the received signals after matched-filtering. The x-axis represents lag-time of the matched filter output and not absolute arrival times. These figures show the time dispersion between different arrivals. And, from these matched-filter outputs, an estimate for array tilt is obtained by considering relative delays in the first arrivals along the VA. From these figures it was estimated that the top of the VA was tilted $\approx 7° \pm 1°$ away from the source. This

corresponds to about a 7.6 m displacement in range between the top and bottom hydrophones. A similar analysis of the FM data for October 23, 1997 was performed resulting in an estimate for the tilt of about $3° \pm 1°$ in the same direction which corresponds to about a 3.2 m displacement in range between the top and bottom hydrophones. These tilt values agree in both magnitude and direction with the inverted values.

The second method for estimating tilt was by inference of the measured ocean current magnitude and direction near the VA (currents shown in Fig. 4). Here, a hydro-static model of the VA system is used considering, among other factors, the VA drag and the buoyancy of the sub-surface float [30]. In Fig. 15, the estimated VA shape is shown using measured ocean currents data from October 22-23. These values are slightly lower than those found using the matched-filter response and MFP inverted values. The reason could be underestimation of the drag of the VA and mooring. However, the hydro-static model correctly predicts the direction of tilt and shows the approximate change in tilt between October 22 and 23. The model also gives an impression of the VA shape. The acoustic propagation model always assumes a straight VA even if it is tilted, and from Fig. 15 it seems a reasonable approximation.

4.1.3 Analysis of the geo-acoustic parameter estimates

The geo-acoustic inversion results (Table 4) taken from data at different ranges and frequencies are not entirely in agreement with each other. Complete agreement between the four inversion results would be inconsistent with the known range dependence of the track. Note the value for $c_{1,sed}$ taken from the LF multi-tone signal at 1.5 km range. A much higher sound speed value was found compared with the other inversions. The probable cause is found in the layering of the bottom (refer back to Fig. 9). Near the VA, the first significant layer has thickness of about 6 m (shown as a gray line in Fig. 9). Moving from the VA along the acoustic track, this surface layer decreases in thickness and then increases again. At about 1.5 km from the VA, the layer nearly disappears. At this point, the inversion results show a marked increase for $c_{1,sed}$. Note, however, for the nearby 2.1 km HF inversion the value $c_{1,sed} = 1580$ m/s along with $h_{sed} = 5.7$ m. It is likely that the higher frequency acoustic data inversion is capable of resolving the thin surface layer whereas the low frequency inversion is not. Since the shortest wavelength in the LF inversion is 5 m, it is unlikely that this layer has great influence on acoustic fields at these frequencies. That is, the surface layer is much thicker, with respect to wavelength, for the high frequency signals compared to the low. At 3.5 km, this surface layer becomes thicker, to nearly 10 m, and the value found from the LF inversion there is $c_{1,sed} = 1576$ m/s which is in much better agreement with the 0.7 km HF result of 1580 m/s and the 2.1 km result of 1572 m/s.

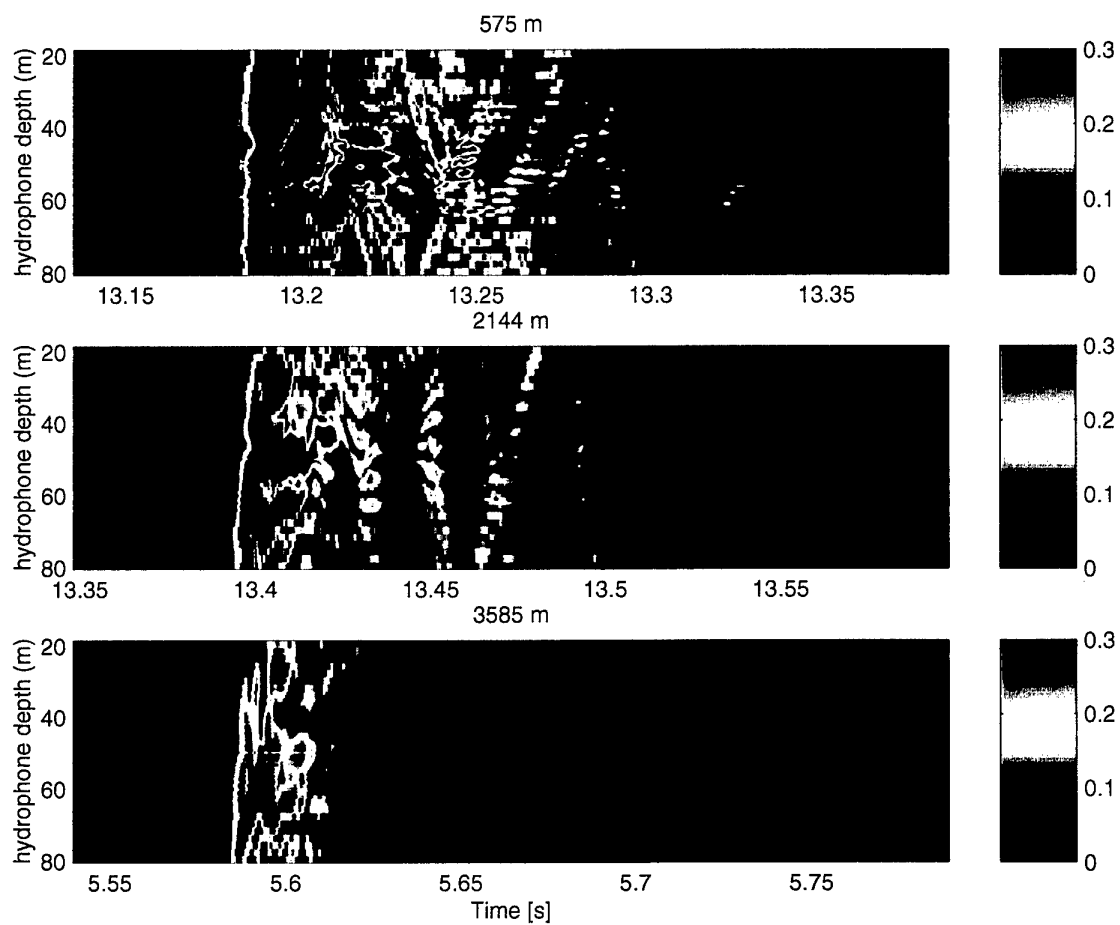Additional support for the inverted values of $c_{1,sed}$ is given by the wide angle reflec-

Figure 14 *The matched-filter outputs for FM's transmitted on October22, 1997 at three different ranges which are indicated at the top of each panel.*
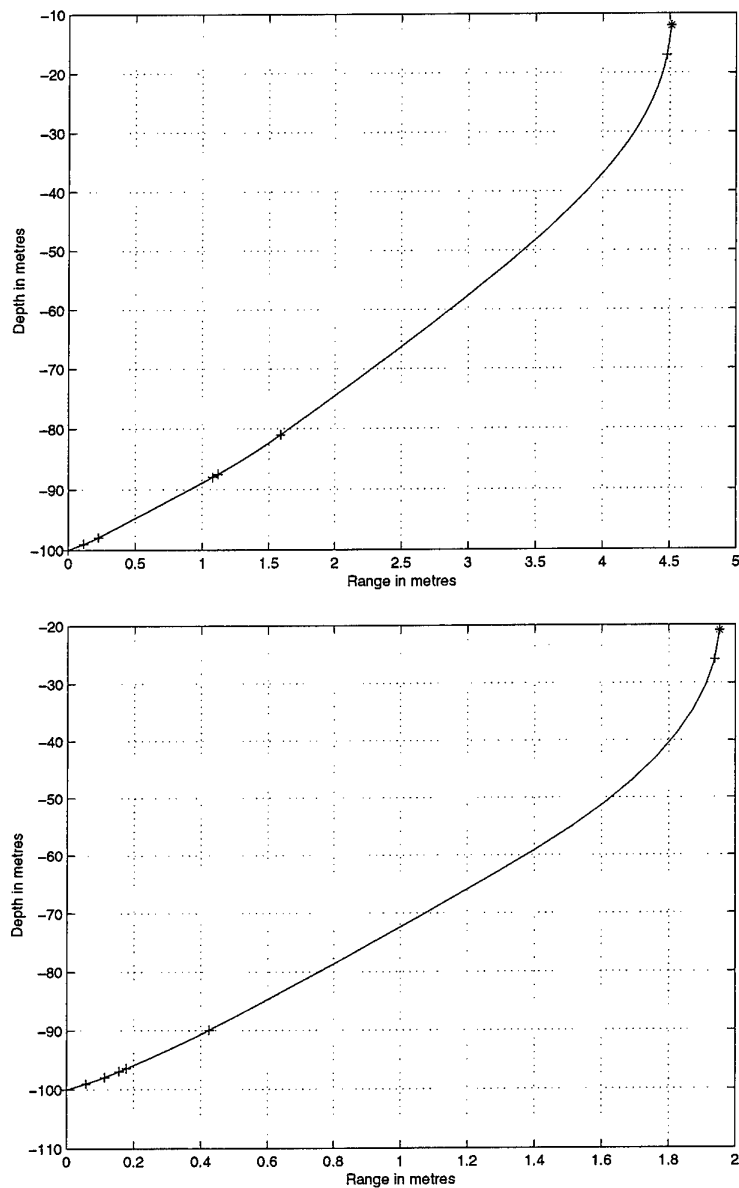
Figure 15 *Estimated VA displacement as a function of depth for October 22 (top) and October 23 (bottom). Star (*) indicates depth of the sub-surface buoy and directly below, the + mark indicates the depth of the shallowest hydrophone and the next + mark indicates the depth of the deepest hydrophone. The lower four + marks indicate link points for VA electronics modules and cables.*

– 30 –

tion results in Section 2.3.1. With wide angle reflection, the average sound speed in the top layers is estimated at points where a strong reflector is identified below. Figure 11 identifies two reflectors at the depths indicated and the corresponding velocities within those layers. The values show variability along the track with average sound speed of 1591 m/s with 32 m/s standard deviation which is in keeping with the MFP inversions. There are notable points along the track with sound speed as low as 1540 m/s and as high as 1650 m/s. The wide angle reflection analysis gives the average speed within the layer which compares well with the MFP results. It is important to note that the wide angle seismic analysis gives layer sound speeds at points along the track. The MFP inversion data may be weighted by the bottom properties near the sound source or VA, but because the propagation is over long ranges in comparison to the wide angle data, it gives a more (range) integrated prediction for the bottom properties.

The inverted values of h_{sed} should be interpreted carefully. The multi-layer structure of the bottom (and the range dependence) is not included in the geo-acoustic model. Therefore, h_{sed} represents a break-point, setting a depth in the bottom below which is considered homogeneous and above which is fit with the sound speed gradient determined by $c_{1,sed}$ and $c_{2,sed}$. At 0.7 km (HF), and at 1.5 km (LF) deeper values are found for h_{sed} compared to 2.1 km (HF) and 3.5 km (LF). There is evidence from the seismic analysis that the top layer is thinner and there are fewer lower layers at the longer ranges. The regions beyond about 2 km may be adequately approximated by setting the "basement" at a lower h_{sed} value. Further analysis of the HF and LF inversion results and the relationship with sediment sound speed and thickness is provided with numerical simulations in Section 4.3.

The attenuation is not extremely well resolved in the inversions here but the results set bounds within 0.4–0.9 dB/λ. Like the sound speeds, the attenuation indicates range dependent properties of the bottom. The 0.7 km and 3.5 km inversion results tend towards an attenuation constant similar to sand materials which has a typical value of 0.8 dB/λ [24]. The lower attenuation value found at 1.5 km is consistent with harder (faster) materials in accordance with the inversion values for $c_{1,sed}$.

The density values do not seem consistent with the range dependent seismic profiles or the material types. This parameter was not well determined in the inversion. The density has a small influence on the acoustic field and is therefore difficult to determine to high precision with this MFP inversion method. For the same reasons it usually has little importance for acoustic prediction.

The overall agreement between the direct measurements and MFP inverted parameter values gives indication that the inversion is of good quality. It is difficult to establish "ground-truth" values for all the bottom properties but the seismic analysis provides supporting evidence that the inverted geo-acoustic parameters are reasonable and consistent. The results indicate bottom properties which are similar to

sand materials over rock. These are in agreement with that expected from looking at archived data (Fig. 1) and other analyses in the Adventure Bank area [31].

4.1.4 Measured and simulated acoustic field comparison

Another check of the quality of the inversion is the direct comparison of the simulated and measured acoustic fields. Fig. 16 shows measured and simulated transmission loss (TL) for one snapshot from each of the 0.7 km HF and 2.1 km multi-tone signals. The simulated TL is taken using the GA_{best} environment determined through inversion. Even though the objective function given by (4) uses normalized complex pressure fields, which is not sensitive to absolute level, the simulated fields compare well with the measured TL. Presented in Fig. 17 are the measured and simulated pressure fields (normalized magnitudes) taken from LF snapshots at 1.5 km and 3.5 km source ranges. These simulated fields also use the environment determined from the GA_{best} for that snapshot of data. The LF source did not have adequate calibration data and these fields are therefore normalized and not on an absolute pressure scale (or TL).

4.1.5 Backpropagation ambiguity surfaces

As a final check of the inversion data, matched field ambiguity surfaces are generated [28]. These surfaces are generated by taking hypothetical source positions at all points within a region of the waveguide and simulating the resulting acoustic field on the VA. Each of the fields are correlated with the measured pressure field according to $1 - E(\vec{m}_{ave})$ where E is taken from (4) and $\vec{m}_{ave}$ is the averaged environment given in Table 4. This is equivalent to a normalized "backpropagation" of the measured pressure field from the VA back into the waveguide using the environment found by inversion. Each pixel in the images can take a value between 0 and 1. If the field re-focuses at the true source location, i.e. have a region with high pixel values with little or no ambiguity, it is an indication that the environment is well characterized for acoustic propagation at those frequencies. The ambiguity surfaces are shown in Fig. 18. There are extremely well focused fields near the true transmission locations. There is a slightly lower objective function value for the 2.1 km-HF transmission but with a maximum near the true source location. There is also more ambiguity (or side lobes) for the 1.5 km and 3.5 km transmissions which is typical for low frequency data.
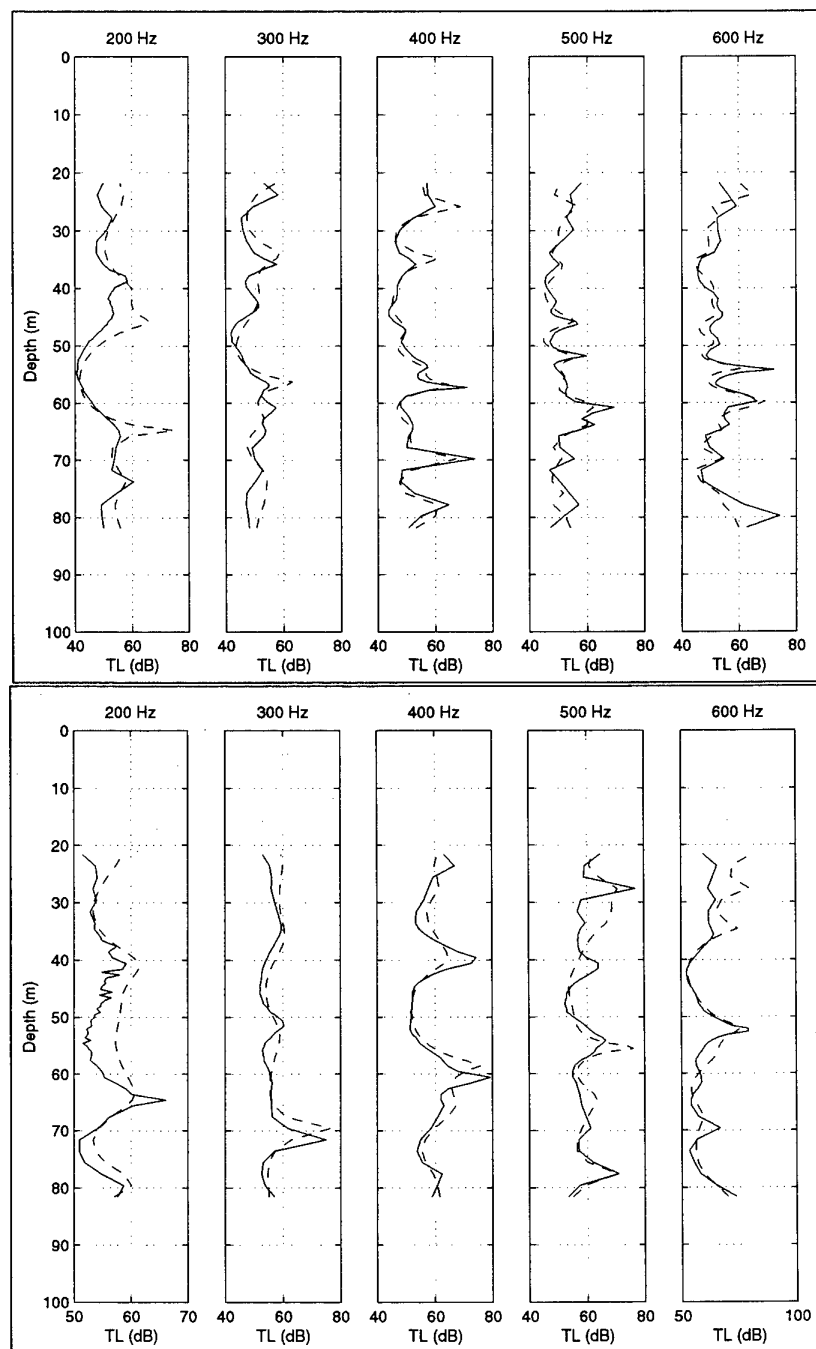
Figure 16 *Experimental (solid) and simulated (dashed) HF transmission loss data along the VA at the indicated frequencies. Top is from 0.7 km source range, bottom from 2.1 km.*
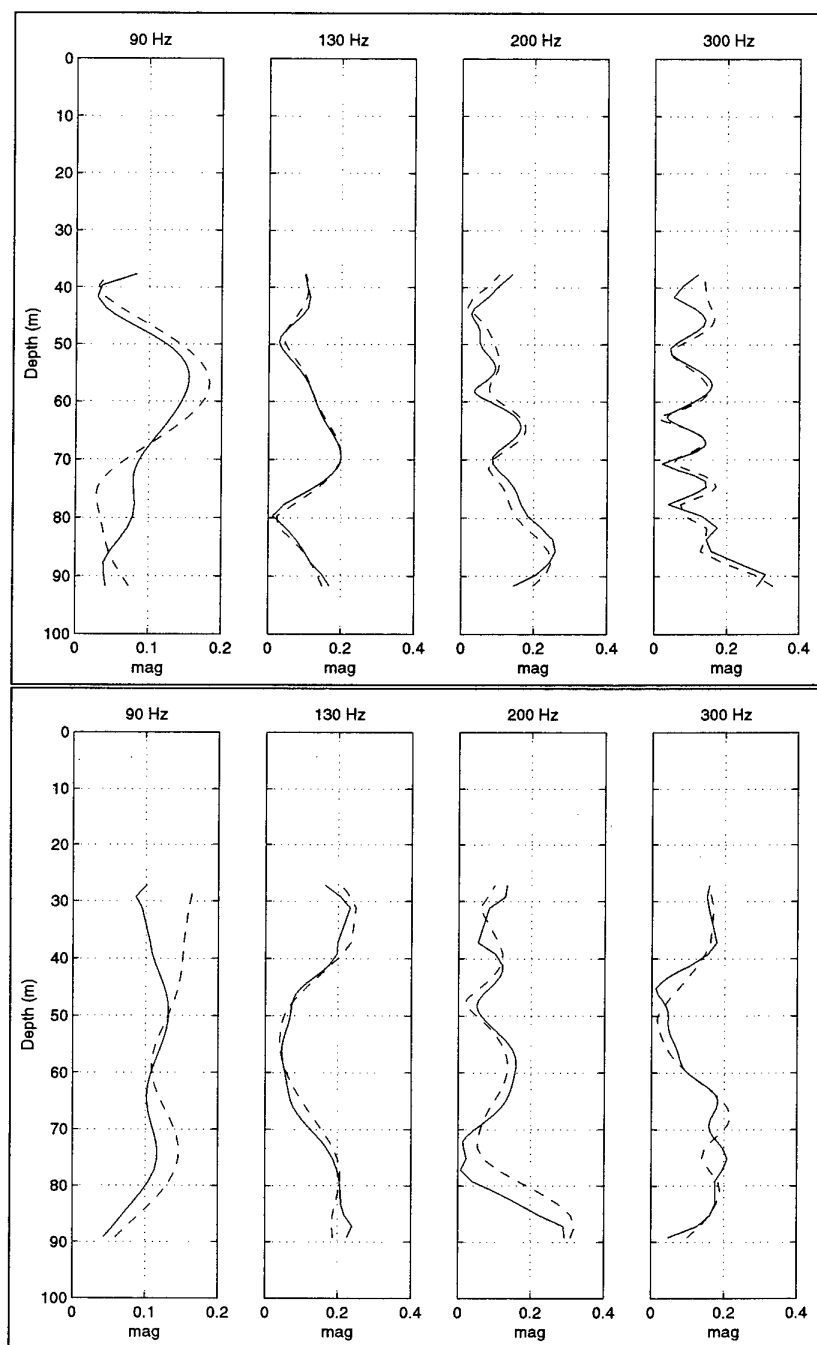
Figure 17 *Experimental (solid) and simulated (dashed) LF pressure field magnitudes along the VA at the indicated frequencies. Top is from 1.5 km source range, bottom is from 3.5 km.*
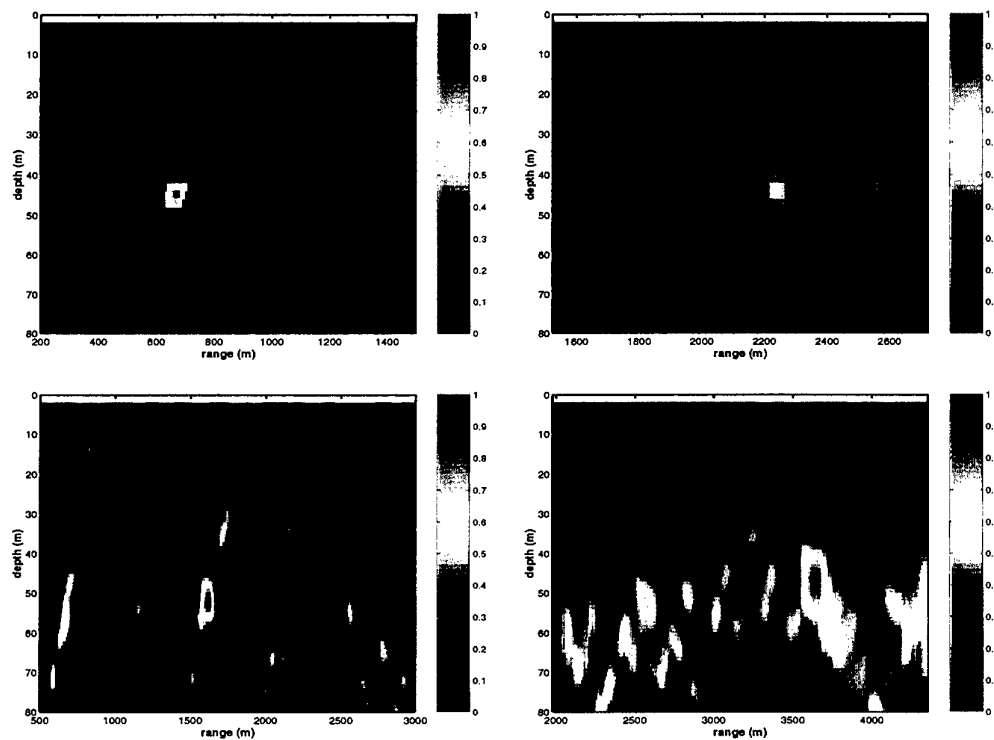
Figure 18 *Ambiguity ("backpropagation") surfaces for one snapshot from each of the four source range positions. Range and depth windows are indicated on the x and y axes. Top left: 0.7 km range position HF transmission. Top right: 2.1 km range position HF transmission. Bottom left: 1.5 km range position LF transmission, Bottom right: 3.5 km range position LF transmission*
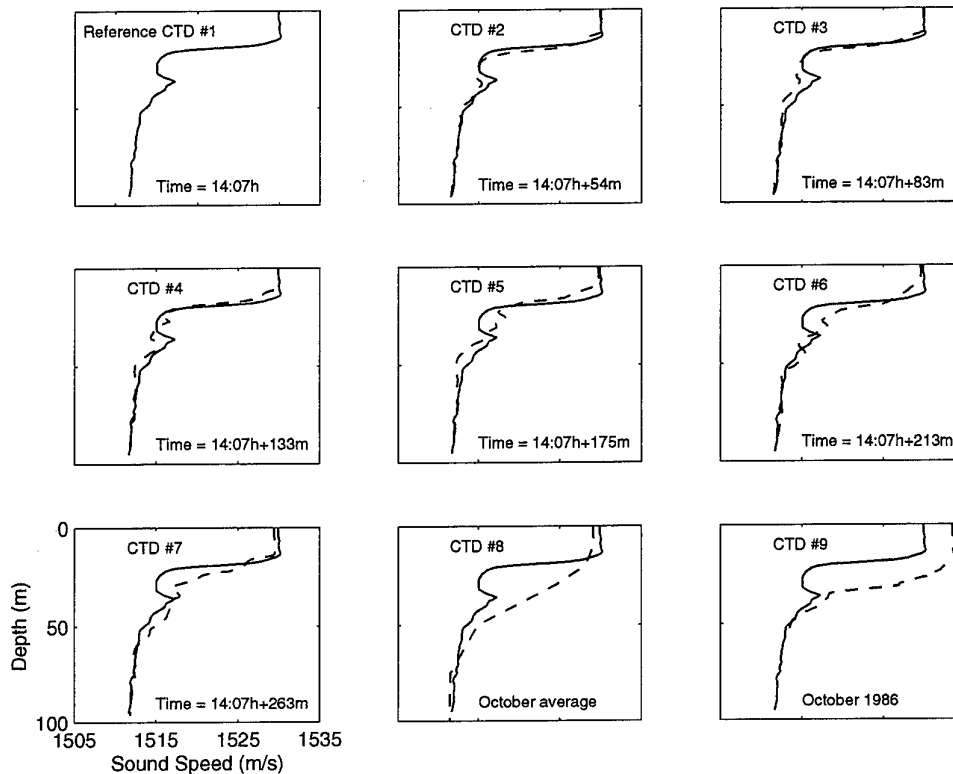
Figure 19 *Sound speeds for Adventure Bank. Top left is the reference profile taken at 14:07 on October 22, 1997 and is shown as a solid line in each of the 9 panels. Sound speeds taken from subsequent CTD casts are shown as dashed lines with times given as minutes after the reference. The archived sound speed taken from the climatology database and profile from October 1986 are also shown as dashed lines in the lowest row right two panels.*

4.2 Effect of sound speed variability on inversion

Studying all the effects of temporal and spatial sound speed variability on propagation and inversion is beyond the scope of this paper. However, some basic analysis is required to make a conclusion about the importance of sound speed on the inversion results. To make this judgment a simple test was made. First, the sound speed labeled Reference CTD#1 in Fig. 19 was used to *simulate* acoustic propagation from a source at 0.7 km and generate reference acoustic data (HF frequencies only). Next, each of the CTD casts taken at different times on that day and shown with dashed lines in Fig. 19, were used as the input to the normal mode forward propagation code as part of a complete inversion using the same method as outlined in Section 3.

Figure 20 shows the final GA_{best} values from these inversions. The top panel gives the final objective function value, eq. (4), and the lower panels give the errors in the final estimation of Δr_s, Δz_s and $\Delta c_{1,sed}$. The solid lines in Fig. 20 are for the *simulated* inversion results for $r_s = 0.7$ km and the dashed line is the same for $r_s = 2.1$ km.

Consider the first seven profiles which are all taken within four hours of the Reference sound speed. These inversion results give final parameter estimates that are within acceptable limits of the known true value. This holds even for the inverted parameters not shown in this figure. As expected, the first inversion which uses the correct sound speed finds all parameters with little error and the objective function is near zero. For subsequent inversions (2–7), there is a slight degradation of the objective function value but the inverted parameters are found near their true values. Consider now, the results of the inversions using the climatology and the October 1986 profiles (numbers 8 and 9 in Fig. 20). The final parameter estimates are significantly worse. Note, the final objective function value is nearly the same for the 2.1 km inversion using profile 7, in comparison with the 0.7 km inversion using the climatology profile 8. Even with almost identical objective function values, the inversion results are, for $c_{1,sed}$, much worse when the climatology profile is used. This suggests how difficult it can be to just use the objective function value for estimating the quality of the inversion results.

4.3 Layer speed and thickness sensitivity

The differences found between some of the inversion results, has been conjectured here as primarily due to the range dependence of the sea-bed. Consider again, the differences in the inversion results for parameter $c_{1,sed}$ taken from the 0.7 km HF and 1.5 km LF data sets. As a sediment layer becomes thin, the acoustic inversion is less sensitive to it. This is exaggerated at lower frequencies as the ratio between layer thickness and acoustic wavelength becomes smaller. A *simulated* HF and LF inversion was made using the geo-acoustic model of Adventure Bank and the same search bounds and method outlined in Section 3. Table 5 gives the inversion results. Only the geo-acoustic parameters are listed as the geometrical parameters were very well determined and are of less interest here.

Some observations can be made from these simulations. If the sediment layer becomes thin especially when there is a large sound speed gradient, there can be significant differences in sound speed estimates between HF and LF inversions. However, significant differences between HF and LF inversions as shown in Table 5 were eliminated when h_{sed} was increased to 20 m (not shown in Table 5). It is likely that with the measured data inversions, something similar to these simulations is occurring. Recall in Fig. 9 at range near 1.5 km from the VA the top sediment layer thins
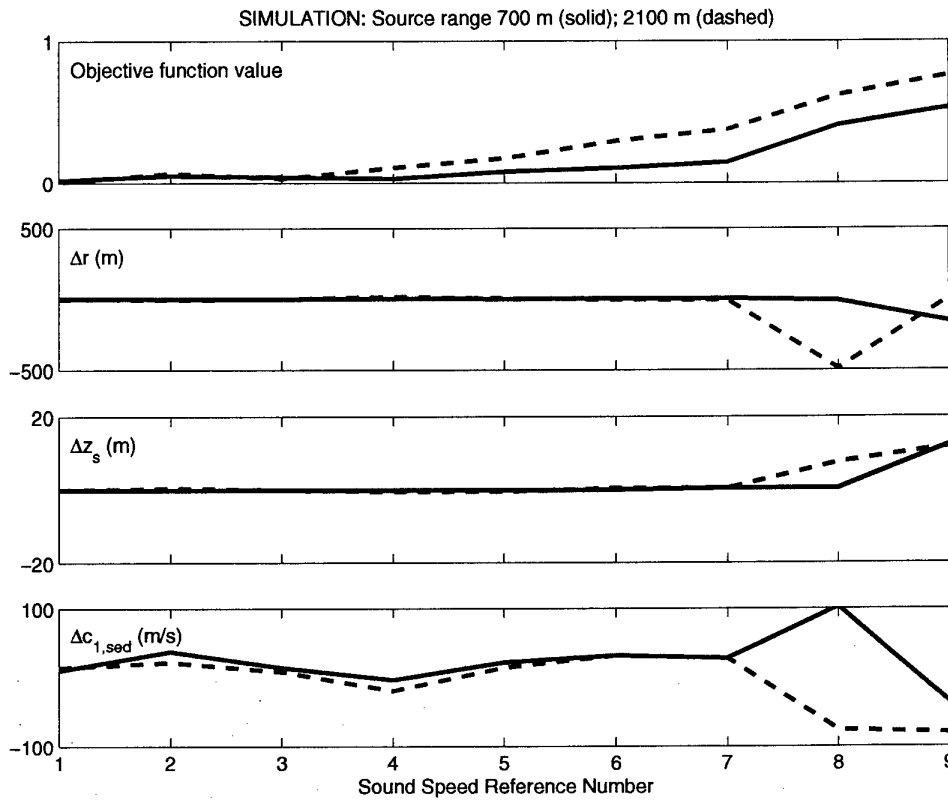
SIMULATION: Source range 700 m (solid); 2100 m (dashed)

Figure 20 *Final (GA_{best}) values from the inversion. The x-axis indicates the sound speed profile Reference number (from Fig. 19) used in the inversion. The top panel gives the final objective function values and below are the errors in estimating r_s, z_s and $c_{1,sed}$. Solid line is taken from simulated inversion results taken for $r_s = 0.7$ km and dashed line for $r_s = 2.1$ km.*

Table 5 *Geo-acoustic parameter values taken from GA_{best} for simulated HF and LF inversions at 0.7 km.*

Range-Band	$c_{1,sed}$ (m/s)	$c_{2,sed}$ (m/s)	c_b (m/s)	h_{sed} (m)	α (dB/λ)	ρ (g/cm^3)
Ground-truth	1572	1790	1812	8.0	0.74	1.43
0.7 km, HF	1595	1771	1799	8.3	0.74	1.44
0.7 km, LF	1675	1752	1864	9.1	0.98	1.42

to a few meters and the reported value for $c_{1,sed}$ and h_{sed} seem to indicate the LF inversion does not sense the top layer. The 2.1 km inversion, however, shows a 5.7 m layer with a strong sound speed gradient. Although the exact parameter values differ between these simulations and the values found by inverting the measured data, the behavior is similar.

5

Conclusions

The EnVerse 97 towed source experiments demonstrated the technique of using acoustic data taken at various source/receiver separations to estimate range dependent properties of the sea-bed. Both high (HF 200-600 Hz) and low frequency (LF 90–300 Hz) bands were used in the inversion. Although the HF and LF data sets were collected on separate days and there was a variable bathymetry which required range dependent forward propagation modeling, these did not pose problems for the inversion. The results are consistent with the bottom layering and sound speeds estimated using standard geo-physical measurements and existing knowledge of the area. A wide angle seismic reflection experiment was conducted using a towed horizontal array to estimate sediment sound speed along the acoustic track. These values agreed with the matched-field processing (MFP) inversion results. A striking feature in the MFP inversion results was $c_{1,sed}$, the sediment sound speed at the water/sediment interface. This parameter changed along the track according to the appearance and disappearance of the surface sediment layer. The jump from 1580 m/s for the HF inversion at 0.7 km to 1641 m/s for the LF inversion at 1.5 km was probably due to a combination of effects. Likely causes are both the thinning layer and the reduced ability to extract the sediment properties due to the lower frequency signals. The combination would act together to increase the sound speed estimate. This calls attention to an important issue in the geo-acoustic inversion. The parameters found which make up the geo-acoustic model are those which can be sensed at the frequencies transmitted. Applying the geo-acoustic parameters to other frequencies may result in erroneous results. Ideally, inverted acoustic data would contain the entire frequency band of interest.

The inverted parameters for the Adventure Bank site were used to simulate acoustic fields which were in excellent agreement with the measured fields. Using the averaged, inverted, geo-acoustic model the "backpropagated" fields correctly localized the position of the source. The genetic algorithm converged and the parameter estimates are reasonably consistent over many snapshots. And, the final inverted geo-acoustic model is consistent with the seismic survey data. Together this indicates the towed source MFP inversion is a promising method for determining geo-acoustic properties over large areas. It was asserted that a relatively recent sound speed profile taken in the vicinity of the experiment should be adequate for the MFP inversion. For inversions taken at longer ranges the sound speed may be more significant. However, archived sound speed profiles did not perform well for either

localization or geo-acoustic inversion. Determining the effects on MFP inversion of stronger range dependence in the water volume and sea-bed are important areas of future research.

Acknowledgments

References

[1] M. D. Collins and W. A. Kuperman, "Focalization: Environmental focusing and source localization," *J. Acoust. Soc. Am.*, vol. 90, no. 3, pp. 1410–1422, 1991.

[2] M. D. Collins, W. A. Kuperman, and H. Schmidt, "Nonlinear inversion for ocean bottom properties," *J. Acoust. Soc. Am.*, vol. 92, no. 5, pp. 2770–2783, 1992.

[3] C. E. Lindsay and N. R. Chapman, "Matched field inversion for geophysical parameters using adaptive simulated annealing," *IEEE Journal of Oceanic Engineering*, vol. 18, no. 3, pp. 224–231, 1993.

[4] S. E. Dosso, M. L. Yeremy, J. M. Ozard, and N. R. Chapman, "Estimation of ocean bottom properties by matched-field inversion of acoustic field data," *IEEE Journal of Oceanic Engineering*, vol. 18, no. 3, pp. 232–239, 1993.

[5] P. Gerstoft, "Inversion of seismo-acoustic data using genetic algorithms and *a posteriori* probability distributions," *J. Acoust. Soc. Am.*, vol. 95, no. 2, pp. 770–782, 1994.

[6] P. Gerstoft, "SAGA Users manual 2.0, an inversion software package," Tech. Rep. SM–333, SACLANT Undersea Research Centre, La Spezia, Italy, 1997.

[7] P. Gerstoft and D. F. Gingras, "Parameter estimation using multi-frequency range-dependent acoustic data in shalow water," *J. Acoust. Soc. Am.*, vol. 99, pp. 2839–2850, 1996.

[8] G. Haralabus and P. Gerstoft, "Source localization in shallow water using multi-frequency processing of shot data," Tech. Rep. SR-253, SACLANT Undersea Research Centre, La Spezia, Italy, 1996.

[9] J. P. Hermand and P. Gerstoft, "Inversion of broadband multi-tone acoustic data from the Yellow Shark summer experiments," *IEEE Journal of Oceanic Engineering*, vol. 21, no. 4, pp. 324–346, 1996.

[10] O. Diachok, A. Caiti, P. Gerstoft, and H. Schmidt, Eds., *Full field inversion methods in ocean and seismo-acoustics*, Kluwer Academic Publishers, Dordrecht, The Netherlands, 1995.

[11] N. R. Chapman and C. E. Lindsay, "Matched-field inversion for geoacoustic model parameters in shallow water," *IEEE Journal of Oceanic Engineering*, vol. 21, no. 4, pp. 347–354, 1996.

[12] A. Tolstoy, "Using matched-field processing to estimate shallow-water bottom properties from shot data taken in the Mediterranean Sea," *IEEE Journal of Oceanic Engineering*, vol. 21, no. 4, pp. 471–479, 1996.

[13] M. Siderius and J. P. Hermand, "Yellow shark spring 1995: Inversion results from sparse broadband acoustic measurements over a highly range-dependent soft clay layer," *J. Acoust. Soc. Am.*, vol. 106, no. 1, 1999.

[14] M. Siderius, D. G. Simons, M. Snellen, J. P. Hermand, and E. van Ballegooijen, "Inversion results from the Enverse 97 shallow water experiments," in *Proceedings of the fourth European conference on underwater acoustics*, Instituto di Acustica, Rome, Italy, 1998, pp. 517–522, Italian National Research Council.

[15] M. Max, N. Portunato, and F. Spina, "Digital map and linked data (DMap) implementation at SACLANTCEN as an aid to sea-going research," SM-291, SACLANT Undersea Research Centre, La Spezia, Italy, 1995.

[16] "Medatlas database," .

[17] W. J. Teague, M. J. Carron, and P. J. Hogan, "A comparison between the Generalized Digital Environmental Model and Levitus climatologies," *J. Geophys. Res.*, vol. 95, no. C5, pp. 7167–7183, 1990.

[18] F. P. Bretherton, R. E. Davis, and C. B. Fandry, "A technique for objective analysis and design of oceanographic experiments applied to MODE-73," *Deep-Sea Res.*, vol. 23, no. 7, pp. 559–582, 1976.

[19] R. Onken and J. Sellschopp, "Seasonal variability of flow instabilities in the Strait of Sicily," *J. Geophys. Res.*, vol. 103, no. C11, pp. 24799–24820, 1998.

[20] A. R. Robinson, J. Sellschopp, A. Warn-Varnas, W. G. Leslie, C. J. Lozano, P. J. Haley Jr., L. A. Anderson, and P. F. J. Lermusiaux, "The Atlantic Ionian Stream," *J. Mar. Systems*, vol. 20, pp. 129–156, 1999.

[21] W. J. Pierson and L. Moskowitz, "A proposed spectral form for fully developed wind seas based on the similarity theory of S. A. Kitaigorodskii," *J. Geophys. Res.*, vol. 69, no. 24, pp. 5181–5190, 1964.

[22] D. J. C. Carter, "Prediction of wave height and period for a constant wind velocity using the JONSWAP results," *Ocean Engineering*, vol. 9, pp. 17–33, 1982.

[23] L. Hatton, M.H. Worthington, and J. Makin, Eds., *Seismic Data Processing, Theory and Practice*, Blackwell Science Ltd., 1986.

[24] F. B. Jensen, W. A. Kuperman, M. B. Porter, and Henrik Schmidt, *Computational Ocean Acoustics*, American Institute of Physics, Inc., New York, 1994.

[25] C. A. Boyles, *Acoustic Waveguides Applications to Oceanic Science*, John Wiley and Sons, Inc., New York, 1984.

[26] M. Siderius, P. Gerstoft, and P. Nielsen, "Broadband geoacoustic inversion from sparse data using genetic algorithms," *J. Comp. Acoust.*, vol. 6, no. 1&2, pp. 117-134, 1998.

[27] A. Tolstoy, N. R. Chapman, and G. Brooke, "Workshop '97: Benchmarking for geoacoustic inversion in shallow water," *J. Comp. Acoust.*, vol. 6, no. 1&2, pp. 1-28, 1998.

[28] A. Tolstoy, *Matched Field Processing for Underwater Acoustics*, World Scientific Pub. Co., River Edge, New Jersey, 1993.

[29] D. G. Simons and M. Snellen, "Multi-frequency matched-field inversion of benchmark data using a genetic algorithm," *J. Comp. Acoust.*, vol. 6, no. 1&2, pp. 135-150, 1998.

[30] L. Troiano, "ETD Cablesim program," Personal communication, June 1999.

[31] A. Caiti, S. M. Jesus, and A. Kristensen, "Geoacoustic seafloor exploration with a towed array in a shallow water area of the Strait of Sicily," *IEEE Journal of Oceanic Engineering*, vol. 21, no. 4, pp. 355-366, 1996.

Document Data Sheet

Security Classification UNCLASSIFIED	Project No. SR-316

Document Serial No. SR-316	Date of Issue September 1999	Total Pages 51 pp.

Author(s)

Siderius, M., Snellen, M., Simons, D., Onken, R.

Title

An environmental assessment in the Strait of Sicily: measurement and analysis techniques for determining bottom and oceanographic properties.

Abstract

In October 1997, the EnVerse 97 shallow water acoustic experiments were jointly conducted by SACLANT Centre, TNO-FEL and DERA off the coast of Sicily, Italy. The primary goal of the experiments was to determine the seabed properties through inversion of acoustic data. Using a towed source, the inversion method is tested at different source-receiver separations in an area with a range-dependent bottom. The sources transmitted over a broad-band of frequencies (90-600 Hz) and the signals were measured on a vertical array of hydrophones. The acoustic data were continuously collected as the range between source and receiving array varied from 0.5-6km. An extensive seismic survey was conducted along the track providing supporting information about the layered structure of the bottom as well as layer sound speeds. The oceanic conditions were assessed using current meters, satellite remote sensing, wave height measurements and casts for determining conductivity and temperature as a function of water depth. Geo-acoustic inversion results taken at different source/receiver ranges show seabed properties consistent with the range dependent features observed in the seismic survey data. These results indicate that shallow water bottom properties may be estimated over large areas using a towed source fixed receiver configuration.

Keywords

Geo-acoustic – inversion – matched field processing – range dependent bottom – towed source – Strait of Sicily – Adventure Bank

The SACLANT Undersea Research Centre provides the Supreme Allied Commander Atlantic (SACLANT) with scientific and technical assistance under the terms of its NATO charter, which entered into force on 1 February 1963. Without prejudice to this main task - and under the policy direction of SACLANT - the Centre also renders scientific and technical assistance to the individual NATO nations.

SACLANT Undersea Research Centre
Viale San Bartolomeo 400
19138 San Bartolomeo (SP), Italy

tel: +39 0187 527 (1) or extension
fax: +39 0187 527 700

e-mail: library@saclantc.nato.int

NORTH ATLANTIC TREATY ORGANIZATION